

ON DISCRETE-CONTINUOUS MODELLING OF THE RAILWAY BOGIE AND THE TRACK FOR THE MEDIUM FREQUENCY DYNAMIC ANALYSIS

T. SZOLC

INSTITUTE OF FUNDAMENTAL TECHNOLOGICAL RESEARCH

POLISH ACADEMY OF SCIENCES

ul. Świętokrzyska 21, 00-049 Warsaw, Poland

e-mail: tszolc@ippt.gov.pl

In the present paper, the dynamic interaction between a bogie of a modern railway passenger car and a track is considered with the aid of a discrete-continuous mechanical model. This model enables us to investigate the bending-torsional-axial vibrations of the wheelsets coupled with the vertical and lateral vibrations of the track through the wheel-rail contact forces. The numerical results are obtained in the form of natural frequencies, eigenfunctions and frequency response functions for the linearized bogie-track system as well as in the form of time histories and corresponding amplitude spectra of forced vibrations obtained by means of computer simulation performed for the non-linear system. In the computational examples for the bogie-track interaction, the influence of static and dynamic properties of several kinds of the track on the system dynamic response is studied.

Keywords: railway bogie-track system, discrete-continuous mechanical model, coupled vertical-longitudinal-lateral-torsional vibrations, numerical simulation.

1. INTRODUCTION

Dynamic investigations of the running gears of modern railway vehicles have been performed for many years by many authors, [1 – 11]. Most of them focused the research on the low frequency range not exceeding 0-30 Hz, in order to study the stability of motion of the railway vehicles and their travel comfort properties, e.g. [1, 2, 6, 9]. The fast development of modern railway vehicles and increasing travelling speeds are associated with the phenomena of early wheel polygonalization and corrugation of rails, generation of the so-called “grumbling”

noise of frequency ca. 100 Hz, as well as of frequently occurring fatigue damages of wheelsets and car suspension elements. These detrimental effects are observed not only in the case of very fast "superexpress" passenger trains, e.g. the ICE trains in Germany or the TGV trains in France, but also in the case of "Inter-City" passenger trains, the travelling speeds of which do not exceed 200 km/h. From practical observations it follows that the above mentioned phenomena result from the dynamic interaction between the wheelsets and the track in the so-called railway medium frequency range between $30 \div 500$ Hz, [7, 8, 10]. In order to find the causes of the "grumbling" noise effects, the phenomenon of wheel polygonalization and of several fatigue defects, it is necessary to introduce an appropriate mechanical model to simulate the process of vehicle-track dynamic interaction. This model must assure a sufficiently accurate representation of all important system properties in the medium frequency range, as well as it should be as simple as possible from the viewpoint of the parameter identification, computational efficiency and ease of interpretation of the obtained results.

In order to achieve this purpose, in [12, 13] a discrete-continuous mechanical model of the single railway wheelset interacting with the track has been applied. By the use of this model in the medium frequency range, the bending-torsional-axial vibrations of the wheelset coupled with vertical-lateral vibrations of the track were investigated. The most severe dynamic response of the considered mechanical system was obtained in the form of parametric resonances for values of the wheelset and the track parameters and for the train speed for which the "grumbling" noise effects are in practice usually observed. In this paper, the considerations are performed for the passenger car entire bogie with two wheelsets interacting with the track. Here, the bogie-track system is also modelled by means of a discrete-continuous model which has been developed from that applied in [12, 13]. By using this model it is possible to investigate, in an effective way, the vertical and lateral vibrations of the track coupled through the contact forces with the bending-torsional-axial vibrations of the bogie wheelsets, running with various speeds on straight and curved tracks of various static and dynamic properties.

2. ASSUMPTIONS

The subject of consideration of the paper is a discrete-continuous mechanical model of a modern passenger car bogie interacting with a track in the medium frequency range. In this model, which is shown in Fig. 1, the wheelset axles are represented by continuous axially rigid and torsionally deformable rotating visco-elastic beams in the form of stepped shafts consisting of several cylindrical segments. The wheels and brake disks are represented by rigid rings attached

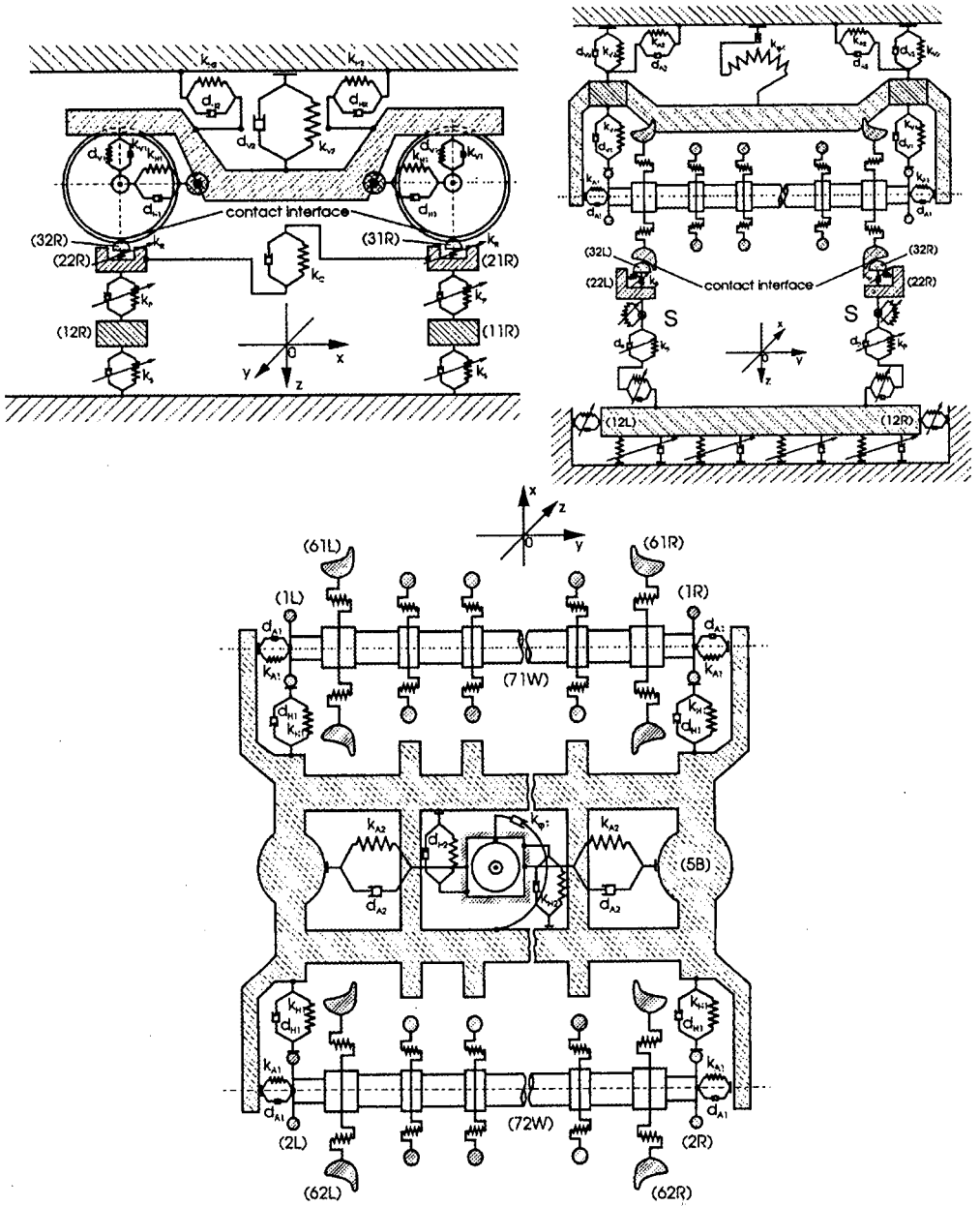


FIG. 1. Discrete-continuous mechanical model of the railway bogie-track system.

to appropriate axle cross-sections by using massless elastic isotropic membranes. These membranes make possible rotations of the rigid rings around their diameters as well as translations along the wheelset axles, Fig. 1. Inertias of the roll bearing housings are represented by the rigid bodies (1L), (2L) and the rigid bodies (1R), (2R) fixed respectively at the left and right ends of the wheelset axles. The wheelset axles are supported at their ends in vertical, longitudinal and axial direction by means of visco-elastic springs corresponding respectively to the vertical, longitudinal and lateral primary suspensions. The bogie frame is represented by a rigid body (5B) of 6 degrees of freedom connected with the car body of infinite inertia by the visco-elastic springs corresponding to the secondary suspension.

The real wheelsets are characterized by brake disks of relatively great axial stiffness in comparison with axial stiffness of the wheels. Thus, for the medium frequency range one can assume infinite axial stiffness of the membranes which connect the rigid rings corresponding to the brake disks with the wheelset axles. According to the above, the lateral vibrations of the bogie are going to be investigated by using the seven-degrees-of-freedom discrete model consisting of the rigid body (5B), the rigid bodies (71W), (72W) representing the entire masses of the wheelset axles and brake disks as well as of the four rigid bodies (61L), (62L), (61R) and (62R) representing masses of the wheels, see Fig. 1. Moreover, according to reality, static and dynamic unbalances of the wheels and brake disks are taken into consideration, which are a source of external excitations.

The real railway track is an endless continuous structure possessing in the vertical and lateral direction periodic properties due to equidistant supports on sleepers. As it follows from [4, 8, 10, 13], in the medium frequency range the track exhibits dynamic properties of the inertial-visco-elastic structure with a clear discrete spectrum of natural frequencies. Separately for the so-called track vertical and lateral dynamics, one can distinguish the first natural frequencies corresponding to the eigenvibration mode, where the rails and the sleepers vibrate "in phase". The second natural frequencies correspond to the eigenvibration mode, where the rails and sleepers vibrate "in anti-phase". The third natural frequencies, both for the track vertical and lateral dynamics, correspond to the so-called "pinned-pinned" mode, for which only the rails vibrate with nodes situated on the sleepers remaining in standstill, [8, 10, 13]. As it follows from [4, 7], the wave propagation velocity in the track is greater than 1000 km/h. Instead of the advanced track models in the form of infinite periodic structures investigated for example in [8, 14], in the medium frequency range for train speeds not exceeding $350 \div 400$ km/h, for a simulation of the dynamic interaction between the flexible wheelsets and the track it seems to be reasonable to introduce a simpler model but characterized by the same or almost the same dynamic properties in

the mentioned range of frequency and train velocities. Thus, in [12] the track has been modelled by the inertial-visco-elastic oscillator of 6 degrees of freedom and in [13] by the inertial-visco-elastic oscillator of 13 degrees of freedom, where in [12] only the vertical dynamics was taken into consideration, and in [13] the vertical-lateral dynamics of the track was investigated. In the both cases such track models created a “dynamic cushion” interacting with a single wheelset. In the case of entire bogie it was assumed that each wheelset interacts with its “own dynamic cushion” represented by the identical inertial-visco-elastic oscillator of 13 degrees of freedom as that in [13]. These “cushions” are mutually coupled in vertical and lateral direction by appropriate springs of stiffness k_{cy} , k_{cl} and k_{ct} , as shown in Fig. 1, where k_{cy} denotes the flexural vertical stiffness, k_{cl} – the flexural lateral one and k_{ct} is the proper rail torsional stiffness. Finally, one obtains the resultant model of the track in the form of dynamic oscillator of 26 degrees of freedom and of periodically fluctuating parameters, in which 12 degrees of freedom describe its vertical dynamics and 14 degrees of freedom describe its lateral dynamics, as one can easily identify from Fig. 1.

For the so-called “small vibrations” it is assumed that free vibrations of the oscillator in the vertical plane are not coupled with the lateral free vibrations. According to the proper assumptions in [12, 13], each “dynamic cushion” for the interaction positions “between the sleepers” and “over the sleeper” must be characterized by the static stiffness values as well as by the dynamic receptance functions, respectively, very close to these obtained from experiments performed on a real track. In the proposed track model in the vertical and lateral direction there are assumed periodically variable stiffness and intensity of damping of the viscous type. The dry friction effects in the subgrade have been omitted. Because during a travel along the real track its dynamic properties vary periodically and continuously from the interaction position “over the sleeper” and “between the sleepers”, [4, 8], in the paper there are assumed two sets of parameters of the oscillator, i.e. masses, damping and stiffness coefficients, separately for the vertical and lateral dynamics each. One set of these parameters represent dynamic properties of the “dynamic cushion” for the interaction position “over the sleeper” and the second one corresponds to the position “between the sleepers”. Both sets of oscillator parameters have been obtained separately for the vertical and lateral dynamics by means of an iterative selection of values of masses, stiffness and damping coefficients, in order to achieve for the three above-mentioned track eigenvibration modes natural frequencies as well as kinetic, potential and dissipation eigenenergies very close to the natural frequencies and eigenenergies, respectively, obtained from experimental measurements performed on a real track, or almost identical to these obtained from proper computations using the more accurate track model in the form of the periodic endless structure, e.g. in [8, 14]. According to the

above, separately for each “dynamic cushion” as well as separately for free vibrations in the vertical and lateral direction, the mass values, stiffness and damping coefficients of the oscillator must satisfy the following approximate relations:

$$\begin{aligned}
 & \frac{1}{2}\omega_m^2 \left[m_{t1}a_{t1m}^2 + 2m_{t2}(a_{t2m} + s_0a_{t4m})^2 + 2m_{t3}(a_{t3m} + s_0a_{t4m})^2 \right. \\
 & \qquad \qquad \qquad \left. + 2m_{t4}a_{t4m}^2 \right] \cong \bar{E}_{Ktm}, \\
 (2.1) \quad & \frac{1}{2} \left[k_{t1}a_{t1m}^2 + 2k_{t2}(a_{t1m} - a_{t2m})^2 + 2k_{t3}(a_{t2m} - a_{t3m})^2 + 2k_{t4}a_{t4m}^2 \right] \\
 & \qquad \qquad \qquad \cong \bar{E}_{Ptm}, \\
 & \frac{1}{2}\omega_m^2 \left[d_{t1}a_{t1m}^2 + 2d_{t2}(a_{t1m} - a_{t2m})^2 + 2d_{t3}(a_{t2m} - a_{t3m})^2 \right. \\
 & \qquad \qquad \qquad \left. + 2d_{t4}a_{t4m}^2 \right] \cong \bar{E}_{Dtm}, \quad m = 1, 2, 3,
 \end{aligned}$$

where ω_m denote the natural frequencies, m_{tj} , k_{tj} , d_{tj} , $j = 1, 2, 3, 4$ are respectively the inertial parameters of the rigid bodies, stiffness and damping coefficients for the vertical dynamics, if the subscript $t = V$, or for the lateral dynamics of the oscillator, if the subscript $t = L$. For vibrations in the vertical and lateral direction, the index $j = 1$ corresponds to the translational motion of the rigid body (1*l*), $j = 2$ to the translational motion of the rigid bodies (2*l*L) and (2*l*R) regarded as one rigid body and the index $j = 3$ corresponds to the translational motion of the rigid bodies (3*l*L) and (3*l*R) regarded also as one rigid body, where $l = 1, 2$ denotes the number of the “dynamic cushion” interacting directly with the l -th wheelset. The index $j = 4$ corresponds to the rigid bodies (2*l*L), (3*l*L) and (2*l*R), (3*l*R) regarded, respectively, as two rigid bodies in simultaneous identical rotational motions with respect to points S , Fig. 1, for the lateral vibrations of the track model. \bar{E}_{Ktm} , \bar{E}_{Ptm} , \bar{E}_{Dtm} are the kinetic, potential and dissipation eigenenergies, respectively, corresponding to the m -th eigenmode of the track estimated by means of proper experimental measurements for the free vertical or lateral vibrations, i.e. for $t = V$ or $t = L$, s_0 is the radius of inertia of the rail cross-section with respect of the rail foot and a_{tim} , $i = 1, 2, 3, 4$, $m = 1, 2, 3$, denote the appropriate eigenvector components. For example, for $t = V$, i.e. for the vertical vibrations it is necessary to assume in (2.1) $a_{V4m} = 0$ and the remaining a_{Vim} correspond to the following eigenmodes: for $m = 1$ all the rigid bodies vibrate “in phase”, for $m = 2$ the rigid bodies (2*l*L), (2*l*R), (3*l*L), (3*l*R) vibrate together “in anti-phase” with respect to the rigid body (1*l*) and for $m = 3$ only the rigid bodies (3*l*L), (3*l*R) vibrate together, when the remaining

rigid bodies are in standstill. For the lateral free vibrations, i.e. for $t = L$, the eigenvector components a_{Lim} correspond to the mentioned successive three eigenmodes in an analogous way as for $t = V$. The two sets of inertial, stiffness and damping parameters for the oscillator selected in this way result separately for the vertical and lateral dynamics each in the following receptance functions corresponding to the interaction position “over the sleeper” and “between the sleepers” shown in Figs. 2 and 3. In Figure 2 there are presented vertical and lateral dynamic receptances for the single “dynamic cushion” compared with the corresponding receptances obtained by means of the measurements performed on the Polish “soft” track of the static average vertical stiffness $0.82 \cdot 10^8$ N/m, the rails of which are supported on wooden sleepers. Figure 3 presents the results of an analogous comparison of the measured and calculated vertical and lateral dynamic receptances for the Polish “hard” track with concrete sleepers and of the static average vertical stiffness $2.03 \cdot 10^8$ N/m. The measurements have been carried out by means of the well known techniques applied e.g. in [8]. To determine the dynamic receptances, the track was excited by hammer impacts. The track static vertical stiffness was sought in the form of a ratio of the known gravitational load imposed on the track to the corresponding measured rail deflection.

The above demonstrated results of track property identification have been obtained under the assumption of track symmetry with respect of its longitudinal axis, which can be imagined as a single “double rail” supported on sleepers. Thus, only the symmetrical eigenmodes have been identified. Identification of the track anti-symmetrical eigenmodes requires further research. The dynamic receptances of the proposed track model can be obtained in the above described way separately for each single “dynamic cushion” or for both the “dynamic cushions” vibrating mutually “in phase”. The relative motions of these “cushions” are, in general, strongly influenced by the coupling stiffness k_{cy} , k_{cl} and k_{ct} , numerical values of which have been also identified experimentally by means of proper comparisons of the corresponding receptances measured directly at the excitation points with these measured at the track points at the distance from the excitation sites equal to the bogie wheelbase value $2b$.

For the track model presented here it is assumed that the values of the determined sets of parameters change periodically and continuously from the set “over the sleeper” to the set “between the sleepers” and then again to the set “over the sleeper” and so on, according to the following function proposed in [4], which is identical for the vertical and lateral dynamics

$$(2.2) \quad p_{li}(t) = \frac{p_{is} + p_{ib}}{2} + \frac{p_{is} - p_{ib}}{2} \left(\cos \left(\frac{2\pi v_0}{l_s} (t - \Delta t_l) \right) + \frac{1}{4} \left(1 - \cos \left(\frac{4\pi v_0}{l_s} (t - \Delta t_l) \right) \right) \right),$$

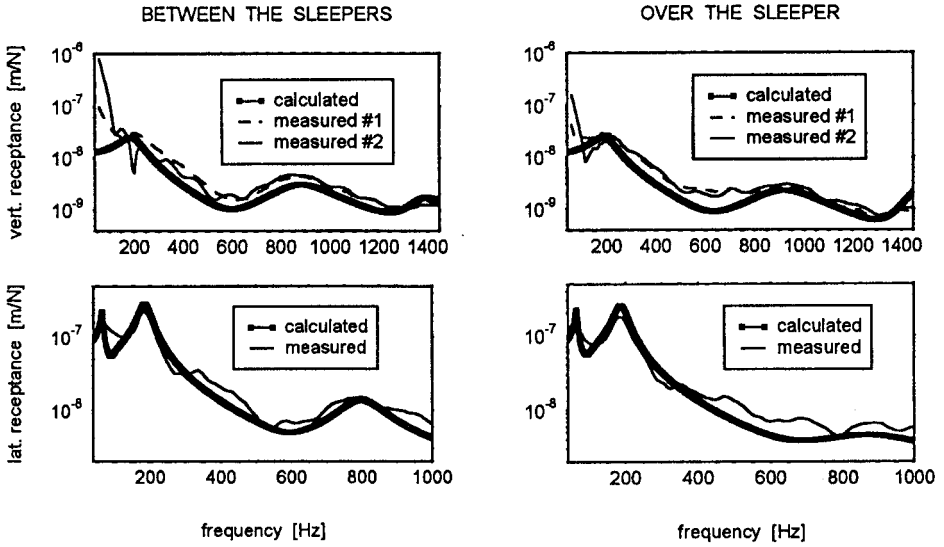


FIG. 2. Dynamic vertical and lateral receptances for the “soft” track.

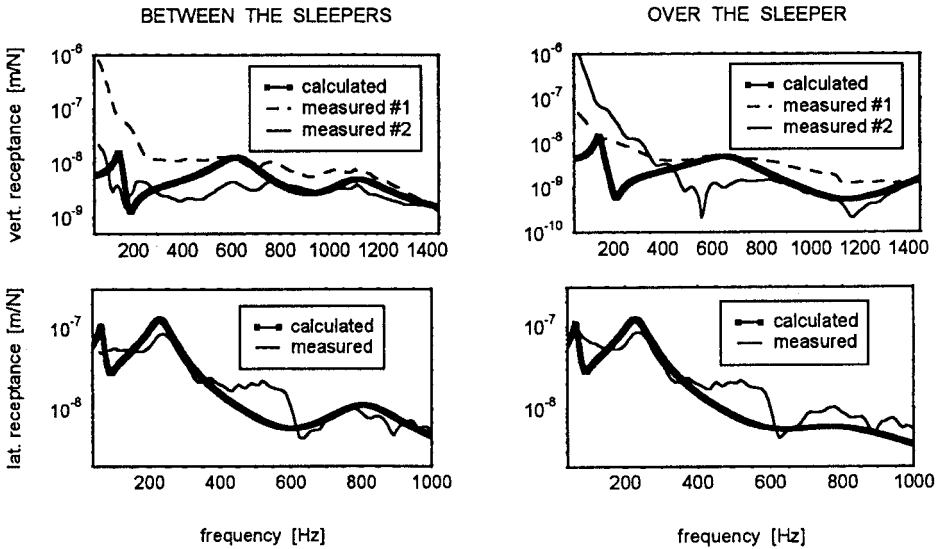


FIG. 3. Dynamic vertical and lateral receptances for the “hard” track.

where $i = 1, 2, 3, 4$, $l = 1, 2$, $\Delta t_1 = -\frac{1}{2v_0} (2b - (\text{entier}(2b/l_s)) \cdot l_s)$, $\Delta t_2 = -\Delta t_1$, and for the l -th "dynamic cushion", $p_{li}(t)$ denotes the i -th particular mass, stiffness or damping parameter of the oscillator, v_0 is the train speed, t denotes time, l_s is the sleeper spacing, $2b$ is the bogie wheelbase and the subscripts s and b denote the receptance positions "over the sleeper" and "between the sleepers", respectively. In the longitudinal direction the track is assumed to be rigid.

The bogie with ideally round wheels running along the straight or circularly curved track with perfectly even rails and without any turnouts or frogs is considered. The wheel tread is assumed to be conical from the outer edge y_e to the cross-section y_f , where the conicity passes into the flange fillet, as shown in Fig. 4 for the right wheel. Thus, a single-point contact as well as an elliptical contact area between the rail head and wheel tread will arise. The rigid bodies $(3lL)$ and $(3lR)$, $l = 1, 2$, of the track model are connected with the rigid rings corresponding to the respective wheelset wheels by means of non-linear visco-elastic springs creating the bogie-track contact interface, Fig. 1. The spring characteristics depend on the applied wheel-rail contact theory. In the proposed model for the normal wheel-rail elastic contact the Hertz theory is used. The vertical component of the normal wheel-rail contact stiffness k_{Cp} is then expressed as a non-linear function of the temporary normal positive contact force according to the appropriate characteristic presented in [8]. However, for negative wheel-rail normal contact force values, k_{Cp} is assumed equal to zero creating in this way unilateral constraints between the bogie wheelsets and the track. For a position of the wheel-rail contact point in the conical range of the wheel tread, the tangential wheel-rail contact is modelled by means of the longitudinal and lateral contact forces expressed as functions of micro-slips between the wheel and the rail using the non-linear theory of Kalker [5], modified by ZHANG and KNOTHE in [15] for the wheel-rail contact in the wheel flange-fillet.

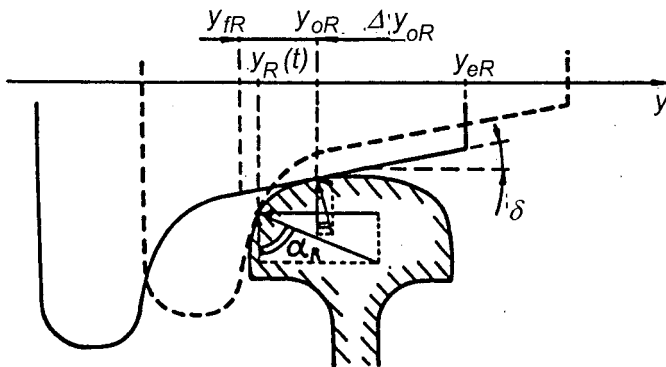


FIG. 4. Contact area of the wheel tread and rail head.

In the paper, for positions of the wheel-rail contact point corresponding to greater wheel cone angles than that of the conical range of the wheel tread $\delta = 0.04 \div 0.05$ rad, i.e. for y smaller than y_f , Fig. 4, the lateral tangential wheel-rail contact forces expressed as micro-slip functions are gradually transformed into lateral forces of the elastic type, i.e. expressed as functions of wheel-rail elastic deflections. Then, the lateral component of the wheel-rail elastic contact stiffness k_{Ap} is assumed in the form of a horizontal projection of the normal stiffness k_{Cp} :

$$(2.3) \quad k_{Ap}(Q_p(t), \Delta y_p(t)) = k_{Cp}(Q_p(t)) \cdot \sin(\arctan(\alpha_p(\Delta y_p(t)) - \tan(\delta)))$$

for $|\Delta y_p(t)| \geq |\Delta y_{0p}|$ and $k_{Ap}(Q_p(t), \Delta y_p(t)) = 0$ for $|\Delta y_p(t)| < |\Delta y_{0p}|$,

where $\alpha_p(\Delta y_p(t)) = \delta \frac{a_p \cdot b_p}{(\Delta y_p(t) - \Delta y_{0p} + a_p) \cdot (\Delta y_p(t) - \Delta y_{0p} + b_p)}$ denotes the derivative with respect of $\Delta y_p(t)$ of the wheel-rail contact point trajectory approximated by means of the analytical function, taking into consideration geometrical shapes of the rail head and wheel tread, $\Delta y_p(t)$ is the lateral relative displacement of the wheel tread and rail head with respect of their mutual nominal position y_{0p} , Fig. 4, $\Delta y_{0p} = y_{0p} - y_{fp}$, δ is the nominal wheel cone angle, t denotes time, the index $p = L, R$ indicates the left- and right-hand wheel/rail, respectively, and a_p, b_p are parameters taking into consideration geometrical dimensions and shapes of the running profiles of the rail head and wheel tread.

3. FORMULATION OF THE PROBLEM

Further considerations are performed by using the orthogonal non-rotating coordinate system $Oxyz$ moving together with the bogie with the constant train speed v_0 . The coordinate x -axis determines the longitudinal direction along the vehicle motion, the y -axis is parallel to the rotation axes of the undeformed wheelset axles with the origin set at the axle left-hand extreme cross-sections, and the vertical z -axis is directed towards the track foundation, Fig. 1.

The wheelset axles are slender enough to apply the Bernoulli-Euler beam theory for the medium frequency range. The equations describing the vertical and longitudinal motion as well as the torsional motion of cross-sections of the i -th cylindrical segment of the l -th wheelset axle are assumed in the following form:

$$(3.1)_1 \quad EI_i = \left[\frac{\partial^4 v_{li}(y, t)}{\partial y^4} + e \frac{\partial^5 v_{li}(y, t)}{\partial y^4 \partial t} \right] + \rho A_i \frac{\partial^2 v_{li}(y, t)}{\partial t^2} = 0,$$

$$(3.1)_2 \quad G \left[\frac{\partial^2 \theta_{li}(y, t)}{\partial y^2} + \tau \frac{\partial^3 \theta_{li}(y, t)}{\partial y^2 \partial t} \right] - \rho \frac{\partial^2 \theta_{li}(y, t)}{\partial t^2} = 0,$$

where: $v_{li}(y, t) = u_{li}(y, t) + jw_{li}(y, t)$, $j = \sqrt{-1}$, $i = 1, 2, \dots, n + 3$, $l = 1, 2$, $u_{li}(y, t)$ denotes the bending displacement in the vertical direction, $w_{li}(y, t)$ denotes the bending displacement in the longitudinal direction, $\theta_{li}(y, t)$ is the angular displacement with respect of the wheelset rotational uniform motion with the constant velocity Ω , EI_i , denotes the bending stiffness of the i -th axle segment of the cross-section area A_i , and n is the number of brake disks. The material damping in the beams is represented by means of the Voigt model, where e and τ denote the viscosity coefficients for bending and torsion, respectively. From the proper estimations performed in [12, 13] it follows that in the realistic operating conditions, the influence of gyroscopic and axial loads acting on the wheelset axles on their bending vibrations is negligible. Thus, the appropriate gyroscopic and axial load terms in Eqs. (3.1)₁ are omitted.

Equation (3.1)_{1,2} are solved under appropriate boundary conditions which, beyond the respective geometrical conformity conditions for displacements and inclinations, contain linear and non-linear equations of equilibrium for the inertial, elastic, contact, gravitational and external damping forces, support reactions, gyroscopic moments as well as for static and dynamic unbalance forces and moments. The equations for the boundary conditions corresponding to the l -th axle suspension at the left-hand side, Fig. 1, have the following form:

$$(3.2)_1 \quad m_1 \frac{\partial^2 v_{l1}}{\partial t^2} + EI_1 \left(\frac{\partial^3 v_{l1}}{\partial y^3} + e \frac{\partial^4 v_{l1}}{\partial y^3 \partial t} \right) + d_{V1} \operatorname{Re} \left[\frac{\partial v_{l1}}{\partial t} - \frac{dq_L}{dt} + \zeta_l b \frac{d\alpha_B}{dt} \right] \\ + k_{V1} \operatorname{Re} [v_{l1} - q_L + \zeta_l b \alpha_B] + j d_{H1} \operatorname{Im} \left[\frac{\partial v_{l1}}{\partial t} - \frac{dq_L}{dt} \right] \\ + j k_{H1} \operatorname{Im} [v_{l1} - q_L] = 0,$$

$$(3.2)_2 \quad -J_1 \frac{\partial^3 v_{l1}}{\partial y \partial t^2} + EI_1 \left(\frac{\partial^2 v_{l1}}{\partial y^2} + e \frac{\partial^3 v_{l1}}{\partial y^2 \partial t} \right) + j I_{01} \Omega \frac{\partial^2 v_{l1}}{\partial y \partial t} = 0,$$

$$(3.2)_3 \quad -I_{01} \frac{\partial^2 \theta_{l1}}{\partial t^2} - D_1 \frac{\partial \theta_{l1}}{\partial t} + G J_{01} \left(\frac{\partial \theta_{l1}}{\partial y} + \tau \frac{\partial^2 \theta_{l1}}{\partial y \partial t} \right) = 0 \quad \text{for } y = 0.$$

The conformity of displacements and inclinations for the cross-sections to which the wheels and brake disks are attached, i.e. for the "bordering" cross-sections

between the adjacent $(i - 1)$ -th and i -th cylindrical segment of the l -th wheelset axle, are expressed by simple equations:

$$(3.2)_4 \quad v_{l,i-1}(y, t) = v_{li}(y, t), \quad \frac{\partial v_{l,i-1}(y, t)}{\partial y} = \frac{\partial v_{li}(y, t)}{\partial y},$$

$$\theta_{l,i-1}(y, t) = \theta_{li}(y, t) \quad \text{for } y = \sum_{k=1}^{i-1} l_k, \quad i = 2, 3, \dots, n + 3, \quad l = 1, 2.$$

The dynamic boundary conditions for these cross-sections have the following form:

$$(3.2)_5 \quad m_i \frac{\partial^2 v_{li}}{\partial t^2} + EI_i \left(\frac{\partial^3 v_{li}}{\partial y^3} + e \frac{\partial^4 v_{li}}{\partial y^3 \partial t} \right) - EI_{i-1} \left(\frac{\partial^3 v_{l,i-1}}{\partial y^3} + e \frac{\partial^4 v_{l,i-1}}{\partial y^3 \partial t} \right)$$

$$+ k_{Cl_i}(Q_{li}(t)) \cdot (\operatorname{Re}[v_{li}] - z_{3li}) + jF_{11li}(Q_{li}(t)) \cdot \operatorname{Im} \left[\frac{\partial v_{li}}{\partial t} \right]$$

$$+ jr_0 F_{11li}(Q_{li}(t)) \frac{\partial \theta_{li}}{\partial t} = G_{wi} + jF_{10li}(Q_{li}(t))$$

$$+ m_i \varepsilon_{li} \left[\left(\Omega + \frac{\partial \theta_{li}}{\partial t} \right)^2 \exp \left(j \left(\frac{\pi}{2} - \tilde{\Theta}_{li} \right) \right) - \frac{\partial^2 \theta_{li}}{\partial t^2} \exp \left(-j \tilde{\Theta}_{li} \right) \right],$$

$$(3.2)_6 \quad EI_i \left(\frac{\partial^2 v_{li}}{\partial y^2} + e \frac{\partial^3 v_{li}}{\partial y^2 \partial t} \right) - EI_{i-1} \left(\frac{\partial^2 v_{l,i-1}}{\partial y^2} + e \frac{\partial^3 v_{l,i-1}}{\partial y^2 \partial t} \right)$$

$$+ \mu_i \left(\varphi_{li} - \frac{\partial v_{li}}{\partial y} \right) = 0,$$

$$(3.2)_7 \quad J_i \frac{d^2 \varphi_{li}}{dt^2} + \mu_i \left(\varphi_{li} - \frac{\partial v_{li}}{\partial y} \right) - jI_{0i} \Omega \frac{d\varphi_{li}}{dt} - F_{22li}(Q_{li}(t), \Delta y_{li}(t))$$

$$- \frac{d}{dt} \left[jI_{xzli} \frac{d\bar{\varphi}_{li}}{dt} \exp(2j\tilde{\Theta}_{li}) + I_{y_{li}}(t) \left(\Omega + \frac{\partial \theta_{li}}{\partial t} \right) \right] = F_{23li}(Q_{li}(t)),$$

$$\begin{aligned}
(3.2)_8 \quad & GJ_{0,i-1} \left(\frac{\partial \theta_{l,i-1}}{\partial y} + \tau \frac{\partial^2 \theta_{l,i-1}}{\partial y \partial t} \right) - \frac{d}{dt} \left\{ \operatorname{Re}[I_{yli}(t)] \cdot \operatorname{Re} \left[\frac{d\varphi_{li}}{dt} \right] \right. \\
& \left. + \operatorname{Im}[I_{yli}(t)] \cdot \operatorname{Im} \left[\frac{d\varphi_{li}}{dt} \right] + \frac{1}{2} m_i \varepsilon_{li} \left[\frac{\partial v_{li}}{\partial t} \exp(j\tilde{\Theta}_{li}) + \frac{\partial v_{li}}{\partial t} \exp(-j\tilde{\Theta}_{li}) \right] \right\} \\
& - GJ_{0i} \left(\frac{\partial \theta_{li}}{\partial y} + \tau \frac{\partial^2 \theta_{li}}{\partial y \partial t} \right) + I_{0i} \frac{\partial^2 \theta_{li}}{\partial t^2} + r_0 F_{11li}(Q_{li}(t)) \cdot \operatorname{Im} \left[\frac{\partial v_{li}}{\partial t} \right] \\
& + r_0^2 F_{11li}(Q_{li}(t)) \frac{\partial \theta_{li}}{\partial t} = r_0 F_{10li}(Q_{li}(t)),
\end{aligned}$$

where

$$I_{yli}(t) = I_{yzli} \exp \left(j \left(\frac{\pi}{2} - \tilde{\Theta}_{li} \right) \right) + I_{xyli} \exp(-j\tilde{\Theta}_{li}),$$

$$\tilde{\Theta}_{li}(y, t) = \Omega t + \theta_{li}(y, t) + \Delta_{li}, \quad \text{for } y = \sum_{k=1}^{i-1} l_k, \quad i = 2, 3, \dots, n+3.$$

Equations for the boundary conditions corresponding to the l -th axle suspension on the right-hand side have an analogous form as those for the left-hand side,

$$\begin{aligned}
(3.2)_9 \quad & m_{n+4} \frac{\partial^2 v_{l,n+3}}{\partial t^2} - EI_{n+3} \left(\frac{\partial^3 v_{l,n+3}}{\partial y^3} + e \frac{\partial^4 v_{l,n+3}}{\partial y^3 \partial t} \right) \\
& + d_{V1} \operatorname{Re} \left[\frac{\partial v_{l,n+3}}{\partial t} - \frac{dq_R}{dt} + \zeta_l b \frac{d\alpha_B}{dt} \right] + k_{V1} \operatorname{Re}[v_{l,n+3} - q_R + \zeta_l b \alpha_B] \\
& + j d_{H1} \operatorname{Im} \left[\frac{\partial v_{l,n+3}}{\partial t} - \frac{dq_R}{dt} \right] + j k_{H1} \operatorname{Im}[v_{l,n+3} - q_R] = 0,
\end{aligned}$$

$$\begin{aligned}
(3.2)_{10} \quad & -J_{n+4} \frac{\partial^3 v_{l,n+3}}{\partial y \partial t^2} - EI_{n+3} \left(\frac{\partial^2 v_{l,n+3}}{\partial y^2} + e \frac{\partial^3 v_{l,n+3}}{\partial y^2 \partial t} \right) \\
& + j I_{0,n+4} \Omega \frac{\partial^2 v_{l,n+3}}{\partial y \partial t} = 0,
\end{aligned}$$

$$(3.2)_{11} \quad I_{0,n+4} \frac{\partial^2 \theta_{l,n+3}}{\partial t^2} + D_{n+4} \frac{\partial \theta_{l,n+3}}{\partial t} + GJ_{0,n+3} \left(\frac{\partial \theta_{l,n+3}}{\partial y} + \tau \frac{\partial^2 \theta_{l,n+3}}{\partial y \partial t} \right) = 0$$

$$\text{for } y = \sum_{k=1}^{n+3} l_k.$$

In Eqs (3.2)₁ and (3.2)₉ the complex functions $q_p(t) = z_p(t) + jx_p(t)$, $p = L, R$, are generalized co-ordinates describing the motion of the rigid body (5B) representing inertia of the bogie frame, where $z_p(t)$ and $x_p(t)$ denote, respectively, the vertical and longitudinal displacements of its left- and right-hand side, and $\alpha_B(t)$ is the angular coordinate with respect of the axis parallel to the wheelset axles, $\zeta_l = 1$ for $l = 1$ and $\zeta_l = -1$ for $l = 2$. It should be remarked that in Eqs. (3.2)₁ – (3.2)₃ and (3.2)₅ – (3.2)₁₁, arguments of the displacement functions $v_{li}(y, t)$ and $\theta_{li}(y, t)$ have been omitted for convenience. In Eqs. (3.2)₁ – (3.2)₃ and (3.2)₅ – (3.2)₁₁ m_i denote masses of the rigid bodies in the wheelset model and J_i , I_{0i} are their diametral and polar mass moments of inertia, respectively, $i = 1, 2, \dots, n+4$, $l = 1, 2$. The products GJ_{0i} denote the torsional stiffness of the i -th axle segment of length l_i , d_{V1} and k_{V1} are, respectively, the damping and stiffness coefficients of the wheelset vertical primary suspension, d_{H1} , k_{H1} are the damping and stiffness coefficients of the longitudinal primary suspension. The symbols G_{wi} for $i = 2, n+3$ denote the components of the static forces perpendicular to the undeformed wheelset axle, pressing down the wheelset wheels to the rails. Values of these forces are determined by proper assumptions, applied e.g. in [1], for the analysis of motion of the railway vehicle during its run along the straight or circularly curved track with a superelevation. For the remaining i , $G_{wi} = 0$. The symbols D_1 , D_{n+4} denote the coefficients of absolute damping in the wheelset bearings. Angular displacements of the rigid rings representing masses of the wheels and brake disks are in (3.2)₆, (3.2)₇, (3.2)₈ expressed by the complex functions $\varphi_{li}(t) = \phi_{li}(t) + j\psi_{li}(t)$, where $\phi_{li}(t)$ and $\psi_{li}(t)$ denote the angular displacements in the vertical and horizontal plane, respectively. The constants μ_i are the bending stiffnesses of the membranes connecting the rigid rings with the axles. It should be remarked that in contradistinction to the gyroscopic forces omitted in Eq. (3.1)₁, acting on the wheelset axle, the boundary condition (3.2)₇ describes the gyroscopic moments acting on the wheels and brake disks. The dynamic unbalances of the rigid rings are described by the products of inertia I_{xyli} , I_{xzli} , I_{yzli} . The static unbalances are expressed as the radial eccentricities ε_{li} of the rigid ring centers of gravity with the appropriate phase angles Δ_{li} , $i = 2, 3, \dots, n+3$, with regard of the longitudinal x -axis of the assumed coordinate system $Oxyz$, k_{cli} is the variable vertical wheel-rail Hertz's stiffness, and $z_{3li} = z_{3lL}$ for $i = 2$ and $z_{3li} = z_{3lR}$ for $i = n+3$ denote the appropriate generalized coordinates of the track model. The symbols $F_{kli}(Q_{li}(t))$, $k = 10, 11, 22, 23$, denote the non-linear contact functions of the dynamic wheel-rail normal force $Q_{li}(t)$ determined by means of the Kalker's theory, [5, 15]. The expressions describing particular forms of $F_{kli}(Q_{li}(t))$ are derived by means of the fundamental relations for the non-linear theory of Kalker demonstrated in [5, 15], assuming the following forms of micro-slip components:

- for the longitudinal micro-slips:

$$v_{xli} = \frac{1}{v_0} \left(\frac{\partial w_{li}(y, t)}{\partial t} + r_0 \frac{\partial \theta_{li}(y, t)}{\partial t} \right) + \frac{\zeta_i a}{2R_0} \quad \text{for } y = \sum_{k=1}^{i-1} l_k,$$

- for the spin micro-slips:

$$v_{yli} = \frac{1}{v_0} \frac{d(\Delta y_{li}(t))}{dt},$$

- for the spin micro-slips:

$$v_{0zli} = \frac{-\delta_{li}(\Delta y_{li}(t))\zeta_i}{r_0}, \quad i = 2, n+3, \quad l = 1, 2,$$

where

$$\Delta y_{l2}(t) = y_{6lL}(t) - r_0 \phi_{l2}(t) - y_{3lL}(t) - s_0 y_{4lL}(t),$$

$$\Delta y_{l, n+3}(t) = y_{6lR}(t) - r_0 \phi_{l, n+3}(t) - y_{3lR}(t) - s_0 y_{4lR}(t),$$

$$\zeta_2 = -1 \quad \text{and} \quad \zeta_{n+3} = 1,$$

y_{3lL} , y_{4lL} , y_{6lL} , y_{3lR} , y_{4lR} , y_{6lR} denote the appropriate generalized coordinates of the track model and of the rigid rings representing wheels, a denotes the nominal rail spacing, and s_0 is the radius of inertia of the rail cross-section with respect of the rail foot. The track curvature radius R_0 is assumed to be positive for left turns and negative for right turns. Then, the contact functions $F_{kli}(Q_{li}(t))$ are obtained in the following form:

$$F_{11li}(Q_{li}(t)) = \sigma_{li} \frac{GC_{11}}{v_0} K_1 [Q_{li}(t)]^{\frac{2}{3}} \quad \text{for } i = 2, n+3,$$

$$F_{11li}(Q_{li}(t)) = 0 \quad \text{for } i = 3, 4, \dots, n+2,$$

$$F_{10li}(Q_{li}(t)) = \zeta_i \sigma_{li} \frac{GC_{11}a}{2R_0} K_1 [Q_{li}(t)]^{\frac{2}{3}} \quad \text{for } i = 2, n+3,$$

$$F_{10li}(Q_{li}(t)) = 0 \quad \text{for } i = 3, 4, \dots, n+2,$$

$$F_{22li}(Q_{li}(t), \Delta y_{li}(t)) = \sigma_{li} \frac{GC_{22}}{v_0} K_1 \left(r_0 [Q_{li}(t)]^{\frac{2}{3}} + j Q_{li}(t) \right) \cdot \frac{d(\Delta y_{li}(t))}{dt} \\ + r_0 k_{Ali}(Q_{li}(t), \Delta y_{li}(t)) \cdot (\Delta y_{li}(t) - \Delta y_{0i}) \quad \text{for } i = 2, n+3,$$

$$F_{22li}(Q_{li}(t), \Delta y_{li}(t)) = 0 \quad \text{for } i = 3, 4, \dots, n+2,$$

$$F_{23li}(Q_{li}(t)) = -\zeta_i \sigma_{li} \delta_{li}(\Delta y_{li}(t)) \left(GC_{23} K_2 Q_{li}(t) - j \frac{GC_{33} K_3}{r_0} [Q_{li}(t)]^{\frac{4}{3}} \right) \\ \text{for } i = 2, n+3,$$

$$F_{23li}(Q_{li}(t)) = 0 \quad \text{for } i = 3, 4, \dots, n + 2, \quad \zeta_2 = -1 \quad \text{and} \quad \zeta_{n+3} = 1, \quad l = 1, 2,$$

where

$$K_1 = m \cdot n \cdot \left[\frac{3(1 - \bar{\nu}^2)}{E(A + B)} \right]^{\frac{2}{3}}, \quad K_2 = (m \cdot n)^{\frac{3}{2}} \cdot \frac{3(1 - \bar{\nu}^2)}{E(A + B)},$$

$$K_3 = (m \cdot n)^2 \cdot \left[\frac{3(1 - \bar{\nu}^2)}{E(A + B)} \right]^{\frac{4}{3}},$$

$A = 1/r_r$, $B = 1/r_0$, G , E are respectively Kirchhoff's and Young's moduli, C_{11} , C_{22} , C_{23} , C_{33} are the Kalker coefficients, $\sigma_{li} = \sigma_{li}(\nu_{xli}, \nu_{yli}, \nu_{0zli}, Q_{li}(t))$ denote the coefficients expressing the nonlinear Kalker's theory, which are determined using the proper algorithm described in details in [15], r_r denotes the curvature radius of the rail head at the contact point, $\bar{\nu}$ is the Poisson number, and the parameters of the contact ellipses taken from Kalker's tabulation scheme are denoted by m and n , [5]. The lateral wheel-rail contact stiffness k_{Ali} is defined by formula (2.3).

From Eqs. (3.2) it follows that the static and dynamic unbalances described in the boundary conditions as well as the contact forces and moments, couple the bending vibrations of the wheelset axles with the torsional vibrations. Moreover, the contact forces and moments couple the bending vibrations with the axial vibrations of both the wheelsets, and in this way also the vertical vibrations of the track with its lateral vibrations. The motion of the track model and the lateral vibrations of the bogie are governed by the following system of parametric ordinary differential equations which are coupled with Eqs. (3.2)₁, (3.2)₅, (3.2)₇ and (3.2)₉:

$$(3.3) \quad \mathbf{M}_T(v_0t)\ddot{\mathbf{s}}(t) + \mathbf{D}_T(v_0t)\dot{\mathbf{s}}(t) + \mathbf{K}_T(v_0t)\mathbf{s}(t) = \mathbf{R}(t),$$

where

$$\mathbf{s}(t) = \text{col} \left[x_L(t), z_L(t), z_{3iL}(t), z_{2iL}(t), z_{12i}(t), z_{2iR}(t), \right. \\ \left. z_{3iR}(t), z_R(t), x_R(t), \alpha_B(t), y_{4iL}(t), y_{3iL}(t), y_{2iL}(t), y_{l1}(t), y_{2iR}(t), \right. \\ \left. y_{3iR}(t), y_{4iR}(t), y_{5B}(t), y_{6iL}(t), y_{6iR}(t), y_{7iW}(t) \right]$$

and

$$\mathbf{R}(t) = \mathbf{R}(v_{l1}(0, t), v_{l,n+3}(\lambda_{n+4}, t), v_{l2}(\lambda_2, t), v_{l,n+3}(\lambda_{n+3}, t), \varphi_{l2}(t), \\ \varphi_{l,n+3}(t), G_c, F(v_0, R_0)), \quad l = 1, 2, \quad \lambda_k = \sum_{j=1}^{k-1} l_j.$$

In Eqs. (3.3) \mathbf{M}_T , \mathbf{D}_T and \mathbf{K}_T denote respectively the mass, damping and stiffness matrix expressed as periodic functions of the parameters (2.2). The terms $F(v_0, R_0)$ and G_c represent external excitation due to centrifugal forces and the component of the gravitational force parallel to the undeformed wheelset axle, respectively, both acting on one half of the car mass and on the entire mass of the bogie frame during its run along the straight or circularly curved track with a superelevation. The components $x_p(t)$, $z_p(t)$, $p = L, R$, and $\alpha_B(t)$ of vector $\mathbf{s}(t)$ are generalized coordinates describing the vertical and longitudinal motion of the bogie frame, $z_{li}(t)$, $j = 3lL, 2lL, 1lL, 12l, 2lR, 3lR$, are generalized coordinates describing the vertical vibrations of the track model, $y_{lk}(t)$, $k = 4lL, 3lL, 2lL, 1l, 2lR, 3lR, 4lR$, are generalized coordinates describing the lateral vibrations of the track model, and $y_{lm}(t)$, $m = 5B, 6lL, 6lR, 7lW$, are generalized coordinates describing the lateral vibrations of the bogie model, $l = 1, 2$.

3.1. Natural vibration analysis

For the proposed model of the bogie and the track, the results of natural vibration analysis are not only essential for further simulation of forced vibrations, but these results give us a better insight into some qualitative dynamic properties of the investigated system. In order to perform an analysis of natural elastic vibrations, all the forcing, viscous, non-linear and unbalance terms standing in the boundary conditions (3.2) have been omitted. Moreover, the variable components of coefficients (2.2) in the parametric equations (3.3) describing motion of the track model and lateral vibrations of the bogie have been also neglected. Thus, one obtains the boundary conditions for the bogie-track model in the following simplified form:

$$(3.4)_1 \quad m_1 \frac{\partial^2 v_{l1}}{\partial t^2} + EI_1 \frac{\partial^3 v_{l1}}{\partial y^3} + k_{V1} \text{Re} [v_{l1} - q_L + \zeta b \alpha_B] + j k_{H1} \text{Im} [v_{l1} - q_L] = 0,$$

$$(3.4)_2 \quad -J_1 \frac{\partial^3 v_{l1}}{\partial y \partial t^2} + EI_1 \frac{\partial^2 v_{l1}}{\partial y^2} + j I_{01} \Omega \frac{\partial^2 v_{l1}}{\partial y \partial t} = 0,$$

$$(3.4)_3 \quad -I_{01} \frac{\partial^2 \theta_{l1}}{\partial t^2} + G J_{01} \frac{\partial \theta_{l1}}{\partial y} = 0 \quad \text{for } y = 0,$$

$$(3.4)_4 \quad v_{l,i-1}(y, t) = v_{li}(y, t), \quad \frac{\partial v_{l,i-1}(y, t)}{\partial y} = \frac{\partial v_{li}(y, t)}{\partial y},$$

$$\theta_{l,i-1}(y, t) = \theta_{li}(y, t),$$

$$(3.4)_5 \quad m_i \frac{\partial^2 v_{li}}{\partial t^2} + EI_i \frac{\partial^3 v_{li}}{\partial y^3} - EI_{i-1} \frac{\partial^3 v_{l,i-1}}{\partial y^3} + \hat{k}_{Cl_i} (\text{Re} [v_{li}] - z_{3li}) = 0,$$

$$(3.4)_6 \quad EI_i \frac{\partial^2 v_{li}}{\partial y^2} - EI_{i-1} \frac{\partial^2 v_{l,i-1}}{\partial y^2} + \mu_i \left(\varphi_{li} - \frac{\partial v_{li}}{\partial y} \right) = 0,$$

$$(3.4)_7 \quad J_i \frac{d^2 \varphi_{li}}{dt^2} + \mu_i \left(\varphi_{li} - \frac{\partial v_{li}}{\partial y} \right) - jI_{0i} \Omega \frac{\partial \varphi_{li}}{\partial t} = 0,$$

$$(3.4)_8 \quad I_{0i} \frac{\partial^2 \theta_{li}}{\partial t^2} + GJ_{0,i-1} \frac{\partial \theta_{l,i-1}}{\partial y} - GJ_{0i} \frac{\partial \theta_{li}}{\partial y} = 0 \quad \text{for } y = \sum_{k=1}^{i-1} l_k,$$

$i = 2, 3, \dots, n+3,$

$$(3.4)_9 \quad m_{n+4} \frac{\partial^2 v_{l,n+3}}{\partial t^2} - EI_{n+3} \frac{\partial^3 v_{l,n+3}}{\partial y^3} + k_{V1} \text{Re} [v_{l,n+3} - q_R + \zeta b \alpha_B]$$

$+ jk_{H1} \text{Im} [v_{l,n+3} - q_R] = 0,$

$$(3.4)_{10} \quad -J_{n+4} \frac{\partial^3 v_{l,n+3}}{\partial y \partial t^2} - EI_{n+3} \frac{\partial^2 v_{l,n+3}}{\partial y^2} + jI_{0,n+4} \Omega \frac{\partial^2 v_{l,n+3}}{\partial y \partial t} = 0,$$

$$(3.4)_{11} \quad I_{0,n+4} \frac{\partial^2 \theta_{l,n+3}}{\partial t^2} + GJ_{0,n+3} \frac{\partial \theta_{l,n+3}}{\partial y} = 0 \quad \text{for } y = \sum_{k=1}^{n+3} l_k$$

where $l = 1, 2$. Due to the truncation of the parametric, viscous and nonlinear terms describing the unbalances, contact forces and contact moments, the bending, torsional and lateral vibrations of the bogie as well as the vertical and lateral vibrations of the track are mutually decoupled. Thus, as it follows from (3.4), the elastic torsional eigenvalue problem can be solved separately and Eqs. (3.3) have been split into three following subsystems of linearized ordinary differential equations. The first one describes the vertical elastic vibrations of the track:

$$(3.5) \quad \hat{\mathbf{M}}_V \ddot{\mathbf{z}}(t) + \hat{\mathbf{K}}_V \mathbf{z}(t) = \hat{\mathbf{R}}(t),$$

where

$$\mathbf{z}(t) = \text{col} [z_L(t), z_{3lL}(t), z_{2lL}(t), z_{1lL}(t), z_{12l}(t), z_{21R}(t), z_{3lR}(t), z_R(t), \alpha_B(t)],$$

$$\hat{\mathbf{R}}(t) = \text{col} \left[k_{V1}u_{l1}(0, t), \hat{k}_{Cl2}u_{l2}(\lambda_2, t), \hat{k}_{Cl, n+3}u_{l, n+3}(\lambda_{n+3}, t), \right. \\ \left. k_{V1}u_{l, n+3}(\lambda_{n+4}, y) \right],$$

and \hat{k}_{Cli} , $i = 2, n + 3, l = 1, 2$, denotes the mean value of the vertical wheel-rail Hertz stiffness corresponding to the static gravitational load. The symbols $\hat{\mathbf{M}}_V$, $\hat{\mathbf{K}}_V$ represent, respectively, the matrices of inertial parameters of the bogie frame and stiffness coefficients of the bogie vertical secondary suspension as well as of mean values of the mass and stiffness coefficients expressed by the first components of the sums in (2.2) for the vertical track dynamics, i.e. for $t = V$. Eq. (3.5) is coupled with Eqs. (3.4)₁, (3.4)₅ and (3.4)₉. This means that, upon the performed linearization, natural bending vibrations of the wheelsets are still coupled with natural vertical vibrations of the track.

The two next equations describe the lateral natural vibrations of the track and the lateral natural vibrations of the bogie:

$$(3.6)_1 \quad \hat{\mathbf{M}}_L \ddot{\mathbf{y}}_T(t) + \hat{\mathbf{K}}_L \mathbf{y}_T(t) = 0,$$

$$(3.6)_2 \quad \mathbf{M}_W \ddot{\mathbf{y}}_W(t) + \mathbf{K}_W \mathbf{y}_W(t) = 0,$$

where $\mathbf{y}_T(t) = \text{col}[y_{4lL}(t), y_{3lL}(t), y_{2lL}(t), y_{l1}(t), y_{2lR}(t), y_{3lR}(t), y_{4lR}(t)]$, $\mathbf{y}_W(t) = \text{col}[x_L(t), y_{5B}(t), y_{6lL}(t), y_{6lR}(t), y_{7lW}(t), x_R(t)]$, $l = 1, 2$, $\hat{\mathbf{M}}_L$, $\hat{\mathbf{K}}_L$ are matrices of the mean values of mass and stiffness coefficients expressed appropriately by the first components of the sums in (2.2) for the track lateral dynamics, i.e. for $t = L$, and \mathbf{M}_W , \mathbf{K}_W denote the mass and stiffness matrices of the bogie model under the lateral vibrations.

The equations of motion (3.1) are solved by means of the well known separation of variables approach

$$(3.7) \quad v_{li}(y, t) = V_{li}(y) \cdot T(t), \theta_{li}(y, t) = \Theta_{li}(y) \cdot T(t) \quad \text{for} \quad \sum_{k=1}^{i-1} l_k \leq y \leq \sum_{k=1}^i l_k, \\ i = 1, 2, \dots, n + 3,$$

where

$$V_{li}^{IV}(y) - (\chi_i k)^4 V_{li}(y) = 0, \quad V_{li}(y) = U_{li}(y) + jW_{li}(y), \\ \Theta_{li}''(y) + \left(\frac{\omega}{c}\right)^2 \Theta_{li}(y) = 0, \quad \ddot{T}(t) + \omega^2 T(t) = 0$$

and

$$\chi_i = 4\sqrt{\frac{A_i}{I_i}}, \quad k = 4\sqrt{\omega^2 \frac{\rho}{E}}, \quad c = \sqrt{\frac{G}{\rho}}, \quad l = 1, 2.$$

Then, the eigenmode functions are sought in the following form:

$$\begin{aligned}
 V_{li}(y) &= A_{1li} \sin(k_i y) + A_{2li} \cos(k_i y) + A_{3li} \sinh(k_i y) + A_{4li} \cosh(k_i y), \\
 (3.8) \quad \Theta_{li}(y) &= B_{1li} \sin\left(\frac{\omega}{c} y\right) + B_{2li} \cos\left(\frac{\omega}{c} y\right) \quad \text{for } \sum_{k=1}^{i-1} l_k \leq y \leq \sum_{k=1}^i l_k, \\
 & \qquad \qquad \qquad i = 1, 2, \dots, n + 3, \\
 \phi_{li}(t) &= \Phi_{li} \exp(j\omega t), \quad \psi_{li}(t) = \Psi_{li} \exp(j\omega t), \quad z_s(t) = Z_s \exp(j\omega t), \\
 & \qquad \qquad \qquad T(t) = \exp(j\omega t),
 \end{aligned}$$

where

$$\begin{aligned}
 A_{mli} &= A_{mli}^{\text{Re}} + j A_{mli}^{\text{Im}}, \quad k_i = \chi_i k, \quad m = 1, 2, 3, 4, \quad i = 1, 2, \dots, n + 3, \\
 & \qquad \qquad \qquad s = 3lL, 2lL, 11l, 12l, 2lR, 3lR, \quad l = 1, 2.
 \end{aligned}$$

Upon a substitution of the solutions (3.8) into the boundary conditions (3.4), one obtains separate characteristic equations for the considered eigenvalue problems:

$$\begin{aligned}
 (3.9) \quad & \bullet \text{ for natural bending vibrations} \\
 & \qquad \qquad \qquad \mathbf{C}(\omega) \bullet \mathbf{D} = \mathbf{0}, \\
 & \bullet \text{ for natural torsional vibrations} \\
 & \qquad \qquad \qquad \mathbf{E}(\omega) \bullet \mathbf{F} = \mathbf{0},
 \end{aligned}$$

where

$$\begin{aligned}
 \mathbf{C}(\omega) & - \text{ is the characteristic complex matrix } ((8(n + 3) + 17) \\
 & \qquad \qquad \qquad \times (8(n + 3) + 17)),
 \end{aligned}$$

$$\begin{aligned}
 \mathbf{D} &= \text{col}(A_{1l1}, A_{2l1}, A_{3l1}, A_{4l1}, A_{1l2}, A_{2l2}, \dots, A_{3l,n+3}, A_{4l,n+3}, \\
 & \qquad \qquad \qquad Z_{3lL}, Z_{2lL}, Z_{11l}, Z_{12l}, Z_{2lR}, Z_{3lR}, Z_L, Z_R, A_B, X_L, X_R),
 \end{aligned}$$

and

$$\mathbf{E}(\omega) - \text{ is the characteristic real matrix } (4(n + 3) \times 4(n + 3)),$$

$$\mathbf{F} = \text{col}(B_{1l1}, B_{2l1}, B_{1l,2}, B_{2l,2}, \dots, B_{1l,n+3}, B_{2l,n+3}), \quad l = 1, 2.$$

Thus, determination of natural frequencies reduces to searching for the values of ω , for which the characteristic determinants of the matrices \mathbf{C} and \mathbf{E} are equal to zero. The eigenmode functions are then obtained by solving the characteristic equations (3.9). In order to find the natural frequencies and eigenvectors for Eqs. (3.6)₁, (3.6)₂, the respective generalized eigenvalue problems must be solved.

3.2. Forced vibration analysis

For the forced vibration analysis, Eq. (3.1) are solved using the Fourier solutions in the form of series in eigenfunctions obtained by means of the natural elastic vibration analysis. Then, the Fourier solutions applied for the forced vibration analysis have the following form:

$$\begin{aligned}
 u_{li}(y, t) &= \sum_{m=1}^{\infty} U_{lim}(y)\xi_m(t), & w_{li}(y, t) &= \sum_{m=1}^{\infty} W_{lim}(y)\eta_m(t), \\
 z_{lk}(t) &= \sum_{m=1}^{\infty} Z_{lkm}\xi_m(t), \\
 \phi_{lj}(t) &= \sum_{m=1}^{\infty} \Phi_{ljm}\xi_m(t), & \psi_{lj}(t) &= \sum_{m=1}^{\infty} \Psi_{ljm}\eta_m(t), \\
 \theta_{li}(y, t) &= \sum_{m=1}^{\infty} \Theta_{lim}(y)\vartheta_m(t), \\
 z_p(t) &= \sum_{m=1}^{\infty} Z_{pm}\xi_m(t), & \alpha_B(t) &= \sum_{m=1}^{\infty} A_m\xi_m(t), \\
 x_p(t) &= \sum_{m=1}^{\infty} X_{pm}\eta_m(t), & p &= L, R, \quad i = 1, 2, \dots, n + 3, \\
 j &= 2, 3, \dots, n + 3, & k &= 3lL, 2lL, 1lL, 12l, 2lR, 3lR, \quad l = 1, 2,
 \end{aligned}
 \tag{3.10}$$

where for the l -th non-rotating wheelset, i.e. obtained for $\Omega = 0$, $U_{lim}(y)$, $W_{lim}(y)$ denote the eigenfunctions of bending displacements in the vertical and longitudinal direction of the i -th axle segment, and Φ_{ljm} , Ψ_{ljm} are the eigenvector components of the angular displacements in the vertical and horizontal plane of the rigid rings, Θ_{lim} denote the eigenfunctions of torsional displacements of the i -th wheelset axle segment, Z_{lkm} are the eigenvector components for the generalized coordinates describing vertical vibrations of the track model, and Z_{pm} , A_m , X_{pm} denote the eigenvector components for the generalized coordinates describing, respectively, vertical and longitudinal vibrations of the bogie frame. Equations (3.6)₁, (3.6)₂ are transformed into the modal coordinates. Then

$$y_i(t) = \sum_{m=1}^{14} Y_{im}\alpha_m(t), \quad y_j(t) = \sum_{m=1}^7 Y_{jm}\beta_m(t),
 \tag{3.11}$$

where Y_{im}, Y_{jm} , $i = 4lL, 3lL, 2lL, l1, 2lR, 3lR, 4lR$, $j = 5B, 6lL, 6lR, 7lW$, $l = 1, 2$, denote the eigenvector components obtained for natural elastic vibrations in the lateral direction for the track and the wheelset, respectively. The unknown time functions in series (3.10) and (3.11) are sought by using the Lagrange equations of the second order. All the forcing, gyroscopic, viscous, parametric and non-linear terms in the boundary conditions (3.2) and Eqs. (3.3), which were omitted in the natural elastic vibration analysis, are regarded here as concentrated external excitations imposed on appropriate cross-sections of the wheelset axle or on appropriate generalized coordinates of the track and bogie model. The generalized external load $H_m(t)$ for the given external excitation $P(t)$ is determined by means of the virtual work principle, which leads to

$$(3.12) \quad H_m(t) = \frac{E_m}{\gamma_m^2} P(t), \quad m = 1, 2, \dots,$$

where E_m denotes the eigenfunction value equal to $E_m = V_m(y_0)$, if the external excitation $P(t)$ is imposed on the wheelset axle cross-section y_0 , and $V_m(y_0)$ is obtained for $y = y_0$ from (3.9) for bending or torsional motion. If $P(t)$ is imposed on the given generalized coordinate $s(t)$, $E_m = S_m$. The symbols γ_m^2 are the coefficients of orthogonality properties, particular forms of which can be found in the APPENDIX. Then, this approach leads to the system of non-linear and parametric ordinary differential equations for the Lagrange coordinates

$$(3.13) \quad \mathbf{M}(\Omega t, v_0 t) \ddot{\mathbf{r}}(t) + \mathbf{C}(\Omega, \Omega t, v_0 t, \dot{\mathbf{r}}(t), Q(t)) \dot{\mathbf{r}}(t) + \mathbf{K}(v_0 t, r(t), Q(t)) \mathbf{r}(t) \\ = \mathbf{F}(t, \Omega^2, \Omega t, Q(t)),$$

where

$$\mathbf{M}(\Omega t, v_0 t) = \mathbf{M}_0 + \mathbf{M}_u(\Omega t) + \mathbf{M}_r(v_0 t),$$

$$\mathbf{K}(v_0 t, r(t)Q(t)) = \mathbf{K}_0 + \mathbf{K}_r(v_0 t, r(t), Q(t)),$$

$$\mathbf{C}(\Omega, \Omega t, v_0 t, \dot{\mathbf{r}}(t), Q(t)) = \mathbf{C}_0 + \mathbf{C}_g(\Omega) + \mathbf{C}_u(\Omega t) + \mathbf{C}_r(v_0 t, \dot{\mathbf{r}}(t), Q(t)).$$

The symbols \mathbf{M}_0 , \mathbf{K}_0 denote, respectively, the constant diagonal modal mass and stiffness matrices, \mathbf{C}_0 is the constant symmetrical damping matrix and $\mathbf{C}_g(\Omega)$ denotes the anti-symmetrical matrix of gyroscopic effects. The terms of unbalance effects are contained in the symmetrical matrix $\mathbf{M}_u(\Omega t)$ and in the non-symmetrical matrix $\mathbf{C}_u(\Omega t)$. $\mathbf{M}_r(v_0 t)$, $\mathbf{K}_r(v_0 t, r(t), Q(t))$ are symmetrical matrices and $\mathbf{C}_r(v_0 t, \dot{\mathbf{r}}(t), Q(t))$ is the non-symmetrical matrix of the parametric and contact effects from the track, and $\mathbf{F}(t, \Omega^2, \Omega t, Q(t))$ is the external excitation vector due to the rail/wheel tread unevenness, unbalance, contact, gravitational and centrifugal forces. The Lagrange coordinate vector $\mathbf{r}(t)$ consists of subvectors of the unknown time functions $\xi_m(t)$, $\eta_m(t)$, $\vartheta_m(t)$, $\alpha_m(t)$, $\beta_m(t)$ from (3.10)

and (3.11). In order to obtain the system dynamic response, equations (3.13) are solved by means of direct integration. During numerical simulation, current values of the normal wheel-rail contact forces $Q_{l2}(t)$ and $Q_{l,n+3}(t)$, $l = 1, 2$, are determined using the cubic extrapolation method. Because the forced bending, torsional and axial vibrations of the wheelsets are mutually coupled with the forced vertical and lateral vibrations of the track, according to the appropriate solutions (3.10) and (3.11), the total number N of Eqs. (3.13) to be solved is a sum of all considered in the frequency range of interest the bending, torsional and lateral eigenmodes of the bogie model and of all lateral eigenmodes of the track model.

The presented discrete-continuous model of the railway bogie-track system enables us to study qualitative properties of the investigated object by means of a natural vibration analysis as well as it makes possible to obtain dynamic responses by using a numerical simulation of forced vibrations. In particular, solving Eqs. (3.13) by means of proper direct integration technique, one obtains the time histories and amplitudes of the wheel-rail dynamic contact forces and slips, dynamic torques transmitted by the wheelset axles, as well as vibratory displacements, velocities and accelerations of several bogie elements excited by wheelset residual unbalances, rail corrugations, wheel tread polygonalization or by periodic fluctuation of track properties during its run.

3.3. Determination of the frequency response function (FRF)

By means of the proposed discrete-continuous model of the bogie track system, it is possible to perform the qualitative dynamic analysis in the form of natural vibration study for the linearized system, and the quantitative analysis by means of the numerical simulation of nonlinear and parametric vibrations. As it was mentioned in Sec. 3.1, due to the linearization of the considered system, the natural vibration analysis is carried out for the four mentioned above kinds of vibrations separately with neglected damping. In order to investigate sensitivity of the entire bogie-track system to several possible resonances, it seems to be reasonable to perform the qualitative analysis using the frequency response function. In order to obtain the frequency response function for the considered bogie-track system it is necessary to neglect all the wheelset residual unbalances, to assume the wheel-rail tangential contact forces as functions of constant static normal forces, to neglect the periodic fluctuation of track properties, to assume the normal wheel-rail contact stiffness of the Hertz type as constant average values as well as to substitute all external excitations by harmonic ones of the common frequency ω and of unitary amplitudes. Upon such linearization Eqs. (3.13) are reduced to the following form:

$$(3.14) \quad \mathbf{M}\ddot{\mathbf{r}}(t) + \mathbf{C}\dot{\mathbf{r}}(t) + \mathbf{K}\mathbf{r}(t) = \mathbf{F}(\omega t),$$

where the $N \times N$ damping-contact-gyroscopic and stiffness matrices \mathbf{C} and \mathbf{K} , respectively, are constant, and the mass matrix \mathbf{M} becomes constant and diagonal. Then, for the harmonic external excitation with frequency ω one can assume:

$$(3.15) \quad r_i(t) = C_i \cos(\omega t) + S_i \sin(\omega t) \quad \text{and} \quad F_i(\omega t) = \sum_j V_{ij} (F_{C_i} \cos(\omega t) + f_{S_i} \sin(\omega t)),$$

where $\sqrt{f_{C_i}^2 + f_{S_i}^2} = 1$, $i = 1, 2, \dots, N$, C_i, S_i are the unknown coefficients, and V_{ji} denote the appropriate eigenfunction values in which, in the proposed method, all the external excitation terms are developed. Introduction of (3.15) into Eqs. (3.14) leads to the system of $2N$ linear algebraic equations

$$(3.16) \quad \mathbf{H}(\omega) \cdot \mathbf{A} = \tilde{\mathbf{F}},$$

where $\mathbf{H}(\omega)$ is the $2N \times 2N$ inverse frequency response function matrix and

$$\mathbf{A} = \text{col}[C_1, C_2, \dots, C_N, S_1, S_2, \dots, S_N],$$

$$\tilde{\mathbf{F}} = \text{col}[f_{C_1}, f_{C_2}, \dots, f_{C_N}, f_{S_1}, f_{S_2}, \dots, f_{S_N}].$$

According to the applied in the proposed approach Fourier's solutions in the form of series in the eigenfunctions, the proper frequency response functions are sought in the following form:

$$(3.17) \quad h_j(\omega) = \sum_i V_{ij} \sqrt{C_i^2(\omega) + S_i^2(\omega)},$$

where the coefficients $C_i(\omega)$ and $S_i(\omega)$ are obtained by solving Eqs. (3.16) for the required range of frequency ω .

4. NUMERICAL RESULTS

The numerical calculations are performed for parameters characterizing the modern car bogie 25ANa of the European "inter-city" or "euro-city" trains IC/EC interacting with the three types of the track. The first two types have been already mentioned in Sec. 2, i.e. the "soft" track with the average static vertical stiffness $k_{Av} = 0.82 \cdot 10^8$ N/m, and the "hard" one with $k_{Av} = 2.03 \cdot 10^8$ N/m, the dynamic receptances of which are presented in Figs. 2 and 3, respectively.

The third type of the track is the “very hard” one typical for the new German railways called “Neubaustrecken” characterized by the relatively large vertical average stiffness reaching $k_{Av} = 3.0 \cdot 10^8$ N/m. The vertical and lateral dynamic receptances for this type of the track are compared in Fig. 5 with the corresponding receptances presented before in Figs. 2 and 3.

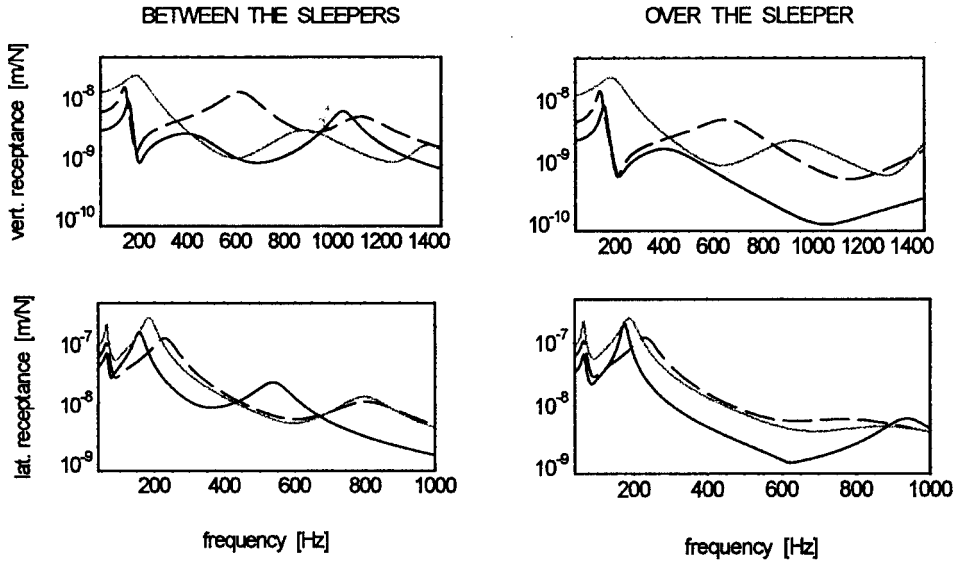


FIG. 5. Comparison of the vertical and lateral dynamic receptances characterizing three railway tracks: the “soft” (—), “hard” (---) and the “very hard” (—) one.

The wheelsets of this bogie possess $n = 2$ brake disks. The static unbalances are assumed, for which: $\varepsilon_{l2} = \varepsilon_{l5} = 1.15 \cdot 10^{-3}$ m and $\Delta_{l2} = \Delta_{l5} = 0$ for the wheels and $\varepsilon_{li} = 1.33 \cdot 10^{-3}$ m and $\Delta_{li} = \pi$ rad, $i = 3, 4$, for the brake disks, $l = 1, 2$. It is assumed that for two identical wheelsets $\varepsilon_{1i} = \varepsilon_{2i}$, $i = 2, 3, 4, 5$, and $\Delta_{1i} = -\Delta_{2i}$, which means that the unbalances of both the wheelsets are mutually oriented in “anti-phase”. Because of typical difficulties in practical identification of the dynamic unbalances of the wheels and brake disks, the corresponding products of inertia I_{yzli} , I_{xyli} , I_{xzli} are assumed to be equal to zero, $i = 2, 3, 4, 5$, $l = 1, 2$.

4.1. Results of the natural vibration analysis

From the viewpoint of dynamic interaction between the railway bogie and the track, some important qualitative characteristics for the vertical and lateral dynamics of the proposed track model have been presented in Sec. 2 and in the introductory part of Sec. 4. To obtain a better insight into the dynamic properties

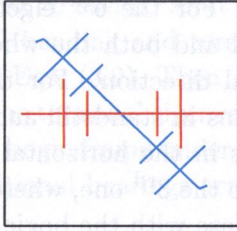
of the considered bogie, in particular in order to investigate its sensitivity to several kinds of vibrations, the natural bending and torsional vibration analysis seems to be useful. As it was mentioned in Subsec. 3.1, for the proposed model, natural bending and torsional elastic vibrations can be analyzed separately by solving Eqs. (3.9). Then, the wheelsets can be regarded as simple torsional trains, when the torsional eigenvalue problem is studied, or as two classical rotors coupled by the bogie frame under bending vibrations, where the track model plays a role of additional bearings acting in the vertical plane only.

The natural bending vibration analysis has been performed for the bogie interacting with the three kinds of the track mentioned above in the frequency range $0 \div 250$ Hz and in the range of wheelset rotational velocity $\Omega = 0 \div 250$ rad/s, in order to investigate an influence of gyroscopic moments on natural frequency values. In Figs. 6a, b there are depicted the eigenmode functions together with the respective natural frequencies obtained for the bogie interacting with the “hard” track for the wheelset rotational velocity $\Omega = 120.8$ rad/s corresponding, at the wheel radius $r_0 = 0.46$ m, to the train speed $v_0 = 55.6$ m/s $\cong 200$ km/h. In these figures the vertical projections of the first wheelset eigenmode functions are plotted by the red lines and their horizontal projections by the blue lines. The vertical projections of the eigenmode functions for the second wheelset are plotted by the green lines and their horizontal projections by the black lines. The left- and right-hand ends of the eigenmode projections of both wheelsets are connected by the bars of the corresponding colors with the points which symbolically visualize the modal displacements of the respective “corners” of the rigid body representing the bogie frame. Thus, one can easily observe the modal motions of the bogie frame with regard of the modal displacements of the wheelsets. From the results of computations it follows that in the investigated frequency range, the bogie-track model possesses 25 eigenmodes of vertical-longitudinal and bending vibrations, while in Figs. 6a, b only 24 of them are shown. The symmetrical structure of the investigated bogie-track system with respect of the track longitudinal axis results in the symmetrical and anti-symmetrical eigenmode functions presented in Figs. 6a, b. As it follows from Fig. 6a, the first nine eigenmodes belonging to the low frequency range $0 \div 30$ Hz are characterized by undeformed or almost undeformed wheelsets. For the 1st eigenmode ($f_1 = 4.441$ Hz), both the wheelsets rotate together around the vertical axis, i.e. they yaw in phase with the bogie frame in the horizontal plane only. For the 2nd eigenmode ($f_2 = 6.624$ Hz) both the wheelsets remain in standstill and only the bogie frame vibrates symmetrically in the vertical direction. For the 3rd eigenmode ($f_3 = 6.950$ Hz) both wheelsets vibrate together symmetrically in phase with the bogie frame in the longitudinal direction only. For the 4th eigenmode ($f_4 = 8.396$ Hz) both wheelsets remain in standstill and only the bogie frame rotates, i.e. it rolls around the track longi-

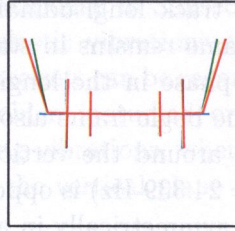
tudinal axis. The 5th eigenmode ($f_5 = 9.403$ Hz) is the pitching one, for which both wheelsets remain in standstill and only the bogie frame rotates around the axis perpendicular to the track longitudinal axis. For the 6th eigenmode ($f_6 = 15.370$ Hz) the bogie frame remains in standstill and both the wheelsets vibrate symmetrically in anti-phase in the longitudinal direction. For the 7th eigenmode ($f_7 = 21.116$ Hz) the bogie frame also remains in standstill and both wheelsets rotate in anti-phase around the vertical axis in the horizontal plane only. The 8th eigenmode ($f_8 = 24.339$ Hz) is opposite to the 3rd one, where both the wheelsets vibrate together symmetrically in anti-phase with the bogie frame in the longitudinal direction only. Similarly, the 9th eigenmode ($f_9 = 26.911$ Hz) is opposite to the 1st one, where both wheelsets together rotate in anti-phase with the bogie frame around the vertical axis in the horizontal plane only. From the numerical calculations performed for the bogie interacting with the “soft” and “very hard” track it follows that in the low frequency range $0 \div 30$ Hz, almost identical results of the natural vibration analysis as these for the “hard” track have been obtained, i.e. almost the same natural frequency values corresponding to the successive nine eigenmode functions presented in Fig. 6a. This means that within $0 \div 30$ Hz, the static and dynamic properties of the railway track do not influence interaction with the bogie, which justifies the assumption of a rigid track model made by many authors investigating the dynamic vehicle-track interaction in the low frequency range, [1, 2, 5, 9]. Moreover, in the low frequency range the computations carried out for other values of the wheelset rotational speed Ω in the interval $0 \div 250$ rad/s have indicated almost no influence of the gyroscopic effects on the natural frequencies and eigenmode functions.

The next 15 eigenmodes belong to the medium frequency range, where the first ones are characterized by the natural frequencies greater than 60 Hz. For all of them, as it follows from Figs. 6a, b, flexural deformations of the wheelset axles are predominant and the bogie frame remains in standstill. Here, both the wheelsets behave as two classical rotors under bending vibrations, which are mutually coupled not by the bogie frame, but by the interaction with the track. Moreover, for the rotating wheelsets the gyroscopic moments couple their motions in the vertical and horizontal plane, which demonstrate the shapes of the all eigenmode functions in Figs. 6a, b, i.e. from the 10th to the 24th. From the computation results it follows that each single wheelset of the bogie demonstrates analogous eigenvibration behavior as the vibrating rotor suspended on the anisotropic supports exhibiting the backward and forward whirl effects described in details in [12, 13]. Also the shapes and natural frequencies of the successive medium frequency eigenmodes are very close or similar to those obtained for a single wheelset in [12, 13]. Nevertheless, it is worth noting that for each backward and forward eigenmode, both the identical wheelsets in the bogie vibrate mutu-

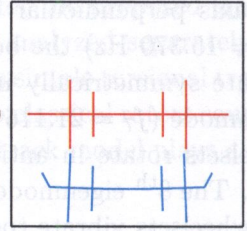
f1 = 4.441 Hz



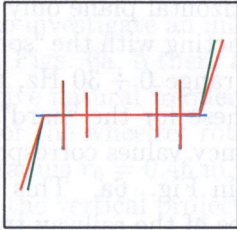
f2 = 6.624 Hz



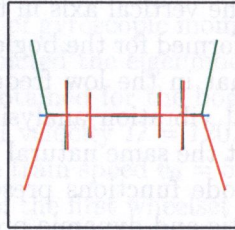
f3 = 6.950 Hz



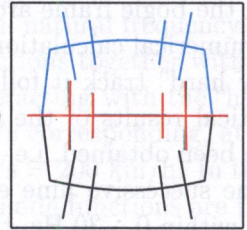
f4 = 8.396 Hz



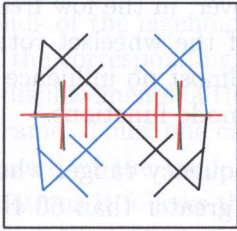
f5 = 9.403 Hz



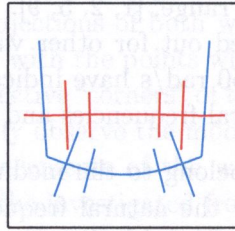
f6 = 15.370 Hz



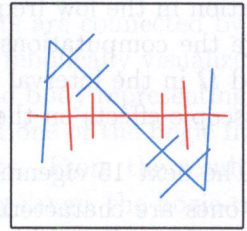
f7 = 21.116 Hz



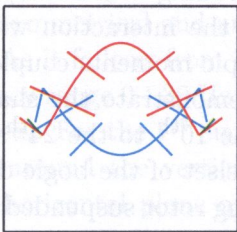
f8 = 24.339 Hz



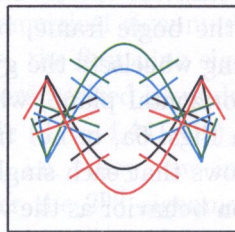
f9 = 26.911 Hz



f10 = 63.435 Hz



f11 = 64.249 Hz



f12 = 71.777 Hz

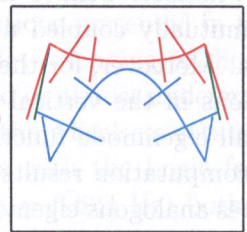


FIG. 6a Bending eigenmode functions and natural frequencies:
 vertical projections for the 1st wheelset (—), horizontal projections for the 1st wheelset (—),
 vertical projections for the 2nd wheelset (—), horizontal projections for the 2nd wheelset (—).

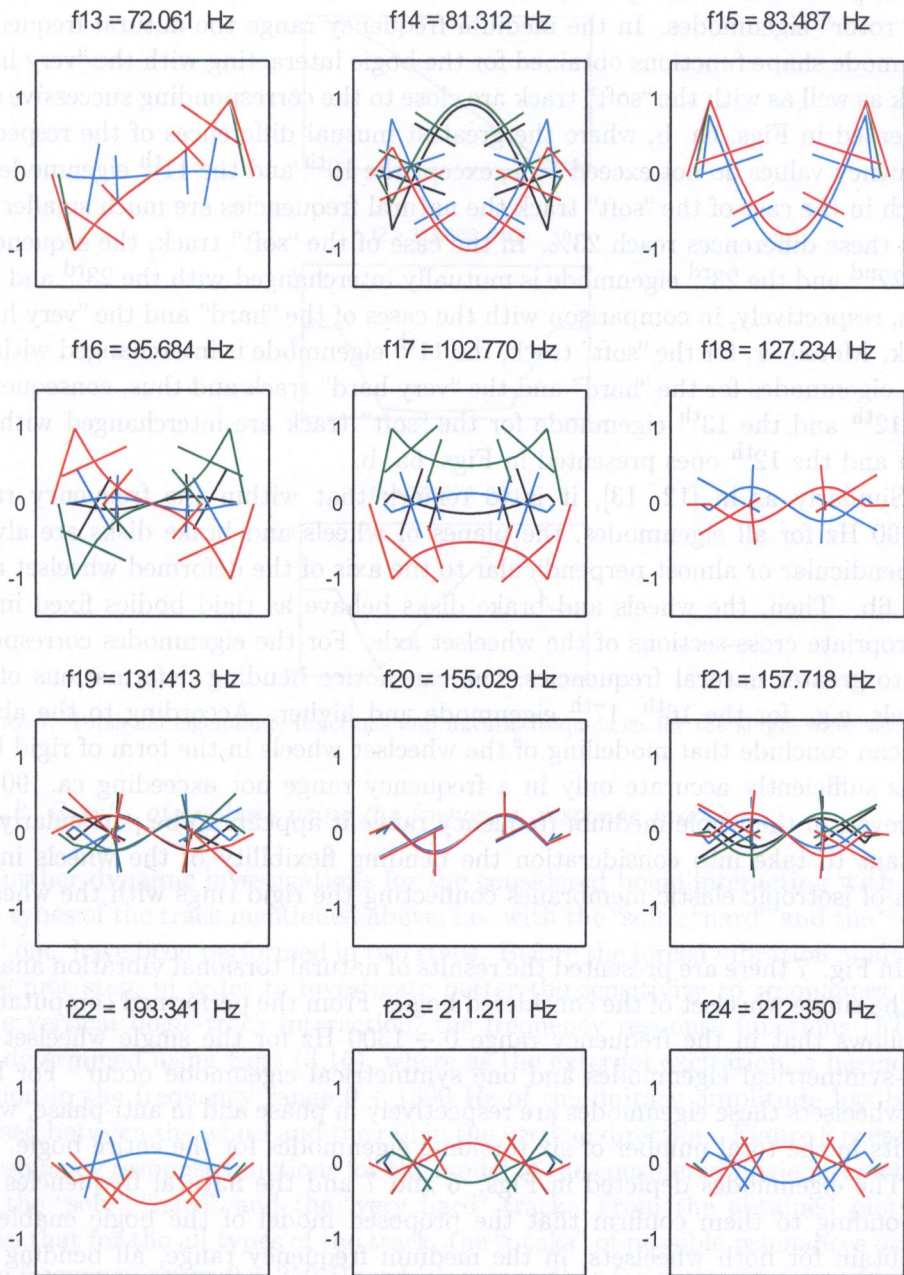


FIG. 6b Bending eigenmode functions and natural frequencies: vertical projections for the 1st wheelset (—), horizontal projections for the 1st wheelset (—), vertical projections for the 2nd wheelset (—), horizontal projections for the 2nd wheelset (—).

ally in phase and in anti-phase, which additionally doubles the entire number of the “rotor” eigenmodes. In the medium frequency range the natural frequencies and mode shape functions obtained for the bogie interacting with the “very hard” track as well as with the “soft” track are close to the corresponding successive ones presented in Figs. 6a, b, where the greatest mutual differences of the respective frequency values do not exceed 15%, except the 10th and the 11th eigenmode, for which in the case of the “soft” track the natural frequencies are much smaller and thus these differences reach 23%. In the case of the “soft” track, the sequence of the 22nd and the 23rd eigenmode is mutually interchanged with the 23rd and 24th ones, respectively, in comparison with the cases of the “hard” and the “very hard” track. Moreover, for the “soft” track, the 11th eigenmode is interchanged with the 13th eigenmodes for the “hard” and the “very hard” track and thus, consequently, the 12th and the 13th eigenmode for the “soft” track are interchanged with the 11th and the 12th ones presented in Figs. 6a, b.

Similarly as in [12, 13], it is to remark that within the frequency range $0 \div 90$ Hz for all eigenmodes, the planes of wheels and brake disks are always perpendicular or almost perpendicular to the axis of the deformed wheelset axle, Fig. 6b. Then, the wheels and brake disks behave as rigid bodies fixed in the appropriate cross-sections of the wheelset axle. For the eigenmodes corresponding to greater natural frequencies, one can notice bending deformations of the wheels, e.g. for the 16th, 17th eigenmode and higher. According to the above, one can conclude that modelling of the wheelset wheels in the form of rigid bodies is sufficiently accurate only in a frequency range not exceeding ca. 90 Hz. However, in the whole medium frequency range it appears to be particularly important to take into consideration the bending flexibility of the wheels in the form of isotropic elastic membranes connecting the rigid rings with the wheelset axle.

In Fig. 7 there are presented the results of natural torsional vibration analysis for the single wheelset of the considered bogie. From the performed computations it follows that in the frequency range $0 \div 1300$ Hz for the single wheelset two anti-symmetrical eigenmodes and one symmetrical eigenmode occur. For both the wheelsets these eigenmodes are respectively in phase and in anti-phase, which results in the total number of six torsional eigenmodes for the entire bogie.

The eigenmodes depicted in Figs. 6 and 7 and the natural frequencies corresponding to them confirm that the proposed model of the bogie enables us to obtain for both wheelsets, in the medium frequency range, all bending and torsional eigenvibration modes as the ones, applied in [3, 4, 10, 11], analogous multi-degree-of-freedom finite element models of the railway single wheelsets.

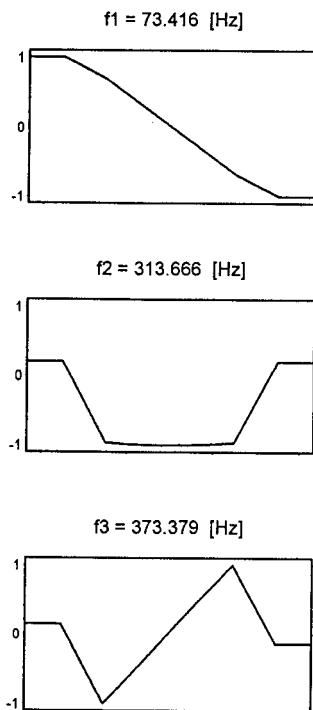


FIG. 7. Torsional eigenmode functions and natural frequencies for the single wheelset.

4.2. Results of analysis using the frequency response function

Further dynamic investigations for the considered bogie interacting with the three types of the track mentioned above, i.e. with the “soft”, “hard” and the “very hard” one, have been performed in two steps. Before the forced vibration analysis, in the first step, in order to investigate better the sensitivity to resonances due to the vertical bogie-track interaction, the frequency response functions (FRF) were determined using Eqs. (3.16), where as the external excitation, a harmonic function in the frequency range $0 \div 1300$ Hz of the unitary amplitude has been imposed between the wheel and the rail in the vertical direction. Figure 8 presents the frequency response functions for the model of the considered bogie interacting with the “soft”, “hard” and the “very hard” track. From the obtained plots it follows that for the all types of the track, the “peaks” of possible resonances occur in the frequency range $0 \div 250$ Hz, which means that for greater frequencies the bogie-track system is not sensitive to vertical excitations from the track, e.g. caused by its unevenness, or due to periodic fluctuation of the track properties during the run. Comparing the frequency response functions plotted in Fig. 8 one can remark that the system bogie-“soft” track is more sensitive to vibrations in

the frequency range $20 \div 100$ Hz, contrary to both the remaining systems, except the local “peak” of the corresponding frequency $82 \div 83$ Hz for the bogie-“hard” track system. In this frequency range the frequency response function for the bogie-“soft” track system is characterized by two resonance “peaks” corresponding to the frequencies 48 and 97 Hz. However, in the frequency ranges $0 \div 20$ Hz and $100 \div 155$ Hz, more sensitive to vibrations excited by the vertical wheel-rail interaction are the systems bogie-“hard” and -“very hard” track. Here, the most severe resonance “peaks” correspond to the frequency of 112 Hz for the bogie “very hard” track system, and to 126 Hz for the bogie “hard” track system, where the latter is significantly greater than the former one because of stronger damping identified in the “very hard” track. Above 155 Hz, all the frequency response functions corresponding respectively to the “soft”, “hard” and the “very hard” track are quite similar to each other, Fig. 8.

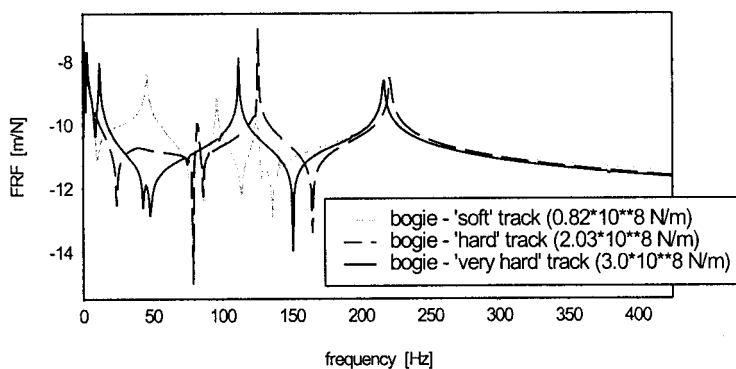


FIG. 8. Frequency response functions of the bogie-track system: for the “soft” (····), “hard” (---) and the “very hard” (—) track.

4.3. Results of the forced vibration analysis

The vertical and lateral track unevenness are usually regarded as fundamental sources of kinematic external excitations of the railway vehicles interacting with the track. For the realistic train travelling speeds, the track unevenness can generate excitations in the low frequency range not exceeding $30 \div 40$ Hz. However, the unevenness of the rail heads and wheel treads in the form of corrugations and wheel polygonalizations are sources of very severe kinematic external excitations in the medium and even high frequency range. The origin of such rail/wheel tread damages are not sufficiently known yet and thus, the primary causes of relatively fast development of rail corrugations and wheel tread polygonalization are still being investigated. According to the above, similarly as for the single wheelset in [12, 13], in this paper the periodic fluctuation of static and dynamic

track properties during run as well as the wheelset residual unbalances are assumed as primary sources of parametric and external excitations for the entire bogie interacting with the track of ideal geometry.

In the second investigation step, the numerical simulations are carried out for the non-linear model of the bogie, i.e. including all the non-linear and parametric terms temporarily neglected in order to determine the frequency response functions. The calculations have been performed for the assumed type of the bogie interacting with the three considered kinds of the track. The fluctuation of track properties during run has been described by the periodic function (2.2). For an appropriate finite number of eigenmodes taken into consideration, a relatively fast convergence of series (3.10) assures a sufficiently accurate solution of Eqs. (3.13). For the investigated mechanical system in the frequency range $0 \div 1300$ Hz 55 bending, 6 torsional and 6 lateral eigenmodes of the bogie as well as 7 lateral eigenmodes of the track have been considered to solve Eqs. (3.13). The studied quantities of interests are the vertical dynamic wheel-rail contact forces, dynamic torques transmitted by the wheelset axles between the wheels and brake disks, tangential wheel-rail relative slips with regard of the full slip in the sense defined in [5, 15] as well as the vertical and longitudinal vibratory displacements of the wheelset wheel geometrical centres in the form of respective orbits. The simulations of bogie-track interaction are performed for various values of the train speed v_0 on the straight and curved track. All these quantities are studied in time and frequency domain.

In Figs. 9 and 10 are presented the results of numerical simulation of the bogie motion on the following straight tracks: on the "soft" track with the travelling speed $v_0 = 58.2$ m/s $\cong 210$ km/h and on the "hard" track with $v_0 = 75.6$ m/s $\cong 272$ km/h. These speed values for the sleeper spacing $l_s = 0.6$ m yield the so-called "track excitation frequencies" equal to $v_0/l_s = 97$ and 126 Hz, corresponding to the most severe peaks of the respective frequency response functions demonstrated in Fig. 8. In Figs. 9 and 10 by black lines there are plotted the responses for the right wheel of the first wheelset of the bogie, by grey lines the dynamic responses for the right wheel of the second wheelset are depicted, and by dashed lines there are denoted the respective static average values. For the straight tracks the assumed symmetrical structure of the considered mechanical system as well as the symmetrical character of the excitations with respect of the track longitudinal axis result in almost identical responses for the left and right bogie wheels, whereas some negligible discrepancies are caused by numerical inaccuracies, which occurred during integration of Eqs. (3.13). Thus, analogous responses of the left wheels of the bogie are not presented in the graphical form.

On the "soft" track for $v_0 = 58.2$ m/s, the periodic variation of the track parameters during run with the track excitation frequency equal to $v_0/l_s = 97$ Hz

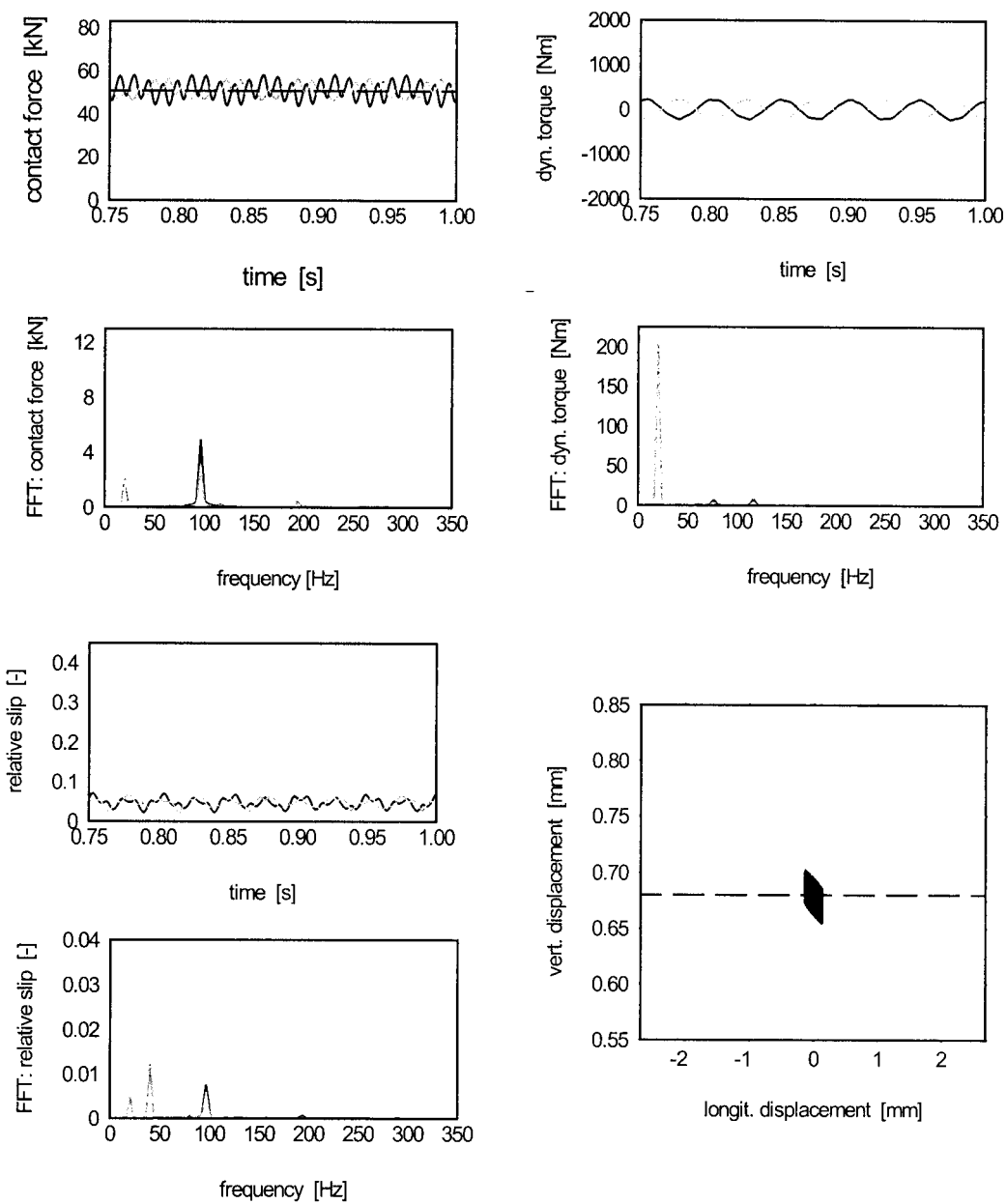


FIG. 9. Dynamic response of the bogie-track system for the straight “soft” track; (—) - for the right-hand wheel of the 1st wheelset, (---) - for the right-hand wheel of the 2nd wheelset, (— — —) - for the static values.

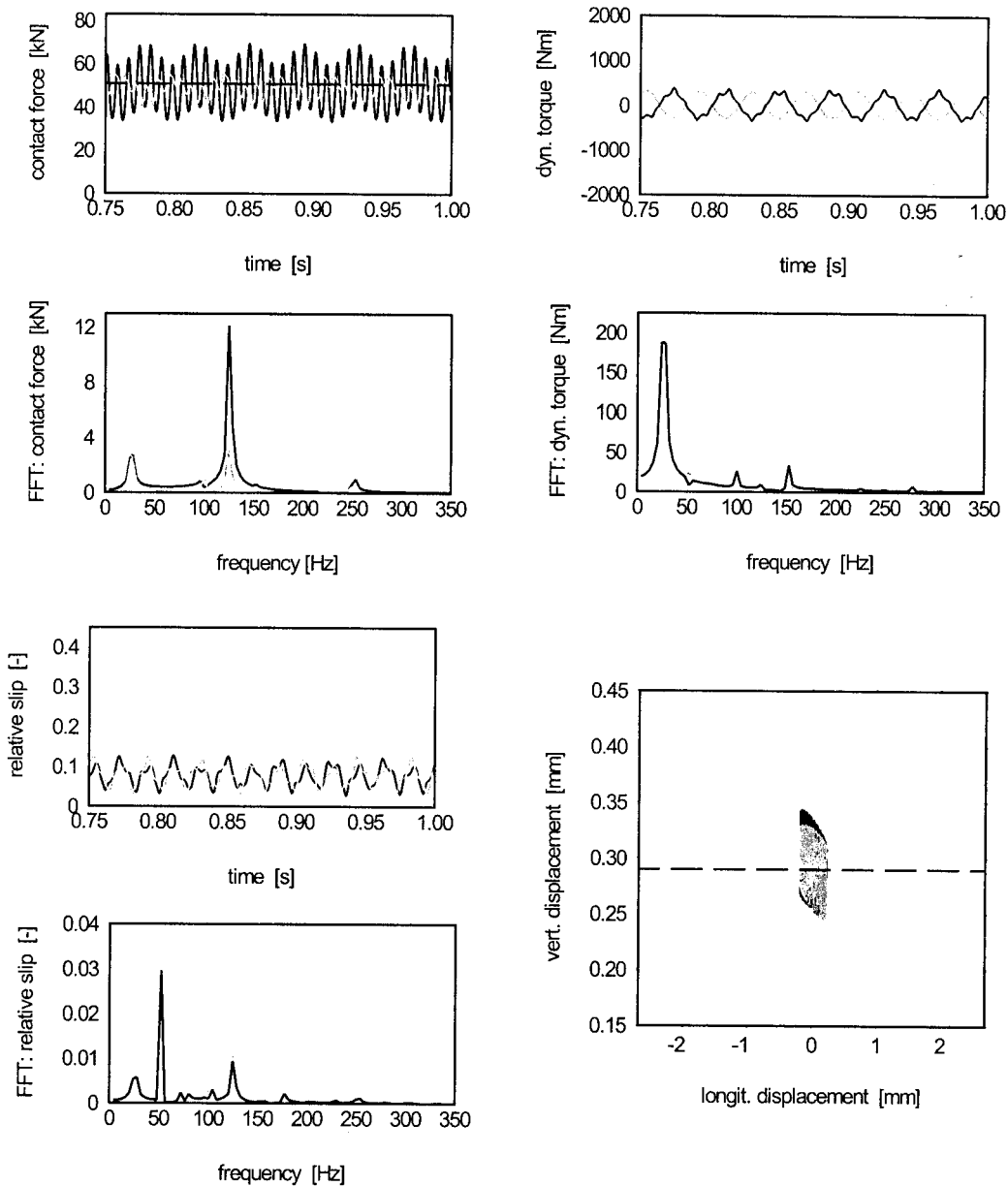


FIG. 10. Dynamic response of the bogie-track system for the straight "hard" track; (—) - for the right-hand wheel of the 1st wheelset, (-----) - for the right-hand wheel of the 2nd wheelset, (— — — —) - for the static values.

results in relatively weak fluctuation of the wheel-rail vertical dynamic contact forces with the fundamental frequency ~ 97 Hz around the gravitational static force, Fig. 9. The amplitudes of these fluctuations do not exceed 14% of the average value, where the contact force amplitudes for the wheels of the first wheelset are slightly greater than those of the second one. The dynamic torques transmitted by the wheelset axles between the wheels and the adjacent brake disks are very similar for both the wheelsets. Their fluctuation amplitudes around zero value are relatively small, i.e. they only slightly exceed 200 Nm with the fundamental frequency ~ 20 Hz corresponding to the unbalance excitation frequency $\Omega/(2\pi) = 20.14$ Hz. From Fig. 9 it follows that the wheel center displacement orbits vary essentially in the vertical direction, where the vibration amplitudes corresponding to the second wheelset are greater than those corresponding to the first wheelset.

In the second case of numerical simulation for the train speed $v_0 = 75.6$ m/s $\cong 272$ km/h on the straight “hard” track, the track excitation frequency $v_0/l_s = 126$ Hz corresponds to the greatest “peak” of the proper frequency response function in Fig. 8. Then, the simulated non-linear response of the bogie-track system is much more severe. The amplitudes of the wheel-rail vertical dynamic contact force fluctuation for the first wheelset reach 38% of the static average value. However, this fluctuation for the second wheelset of the bogie is much smaller, where the corresponding amplitudes do not exceed 18%. Here, at relatively great travelling speed v_0 , the dynamic pressing down of the first bogie wheelset and the dynamic release of the second one are observed. The fluctuations of dynamic torques transmitted by the wheelset axles are in this case also greater, where the amplitudes reach 400 Nm with the fundamental frequency ~ 26 Hz excited by the wheelset unbalances, Fig. 10. The wheel center displacement orbits are characterized by much greater extreme values both in the vertical and longitudinal direction. Greater vertical displacement amplitudes are caused by much stronger, than in the previous case, vertical interaction of the bogie with the track. The much greater amplitudes in the longitudinal direction are a result of more significant influence of excitation due to the wheelset unbalances for the greater speed v_0 and the corresponding to it rotational speed of the wheelset axles Ω .

The numerical simulation has been also carried out for the bogie motion on the “very hard” track with the travelling speed $v_0 = 67.2$ m/s $\cong 242$ km/h yielding the track excitation frequency $v_0/l_s = 112$ Hz corresponding to the most severe “peak” of the respective frequency response function demonstrated in Fig. 8. The obtained results of calculations indicate that in this case, the system dynamic response is qualitatively very similar to that for $v_0 = 75.6$ m/s $\cong 272$ km/h depicted in Fig. 10. The “peak” of the frequency response function for the bogie interacting with the “very hard” track is higher than that for the “soft” track, but

smaller than the greatest “peak” for the “hard” track, Fig. 8. As it follows from the simulated results, the severity of the non-linear response for the bogie interacting with the “very hard” track corresponds to the mutual relations between the compared “peaks” of the frequency response functions. From the appropriate results it follows that the amplitudes of the wheel-rail vertical dynamic contact force fluctuation for the first wheelset reach 25% of the static average value, and for the second one they slightly exceed 20%. In this case the amplitudes of dynamic torques transmitted by the wheelset axles also remain as “middle” values reaching 300 Nm with the fundamental frequency ~ 23 Hz corresponding to the excitation due to the wheelset unbalances with frequency equal to $\Omega/(2\pi) = 23.25$ Hz. In comparison with the wheel center displacement orbits presented in Figs. 9 and 10, the extreme displacements of the orbits obtained for the bogie interacting with the “very hard” track also remain “in the middle” both in the vertical and longitudinal direction because of the mentioned “medium” severity of the vertical bogie-track interaction, as well as since the considered travelling speed value v_0 yields the “medium” wheelset axle rotational speed Ω producing greater unbalance excitations than these in the case of the “soft” track and smaller unbalance excitations than these in the case of the “hard” track.

In the next two computational examples, bogie motion on the curved “hard” track has been simulated. In the first one the motion is assumed on the curved track of curvature radius $R_0 = 4000$ m with the superelevation 0.06 m, with the same travelling speed $v_0 = 75.6$ m/s $\cong 272$ km/h as for the straight track. In the second example the motion is assumed on the curved “hard” track of curvature radius $R_0 = 1800$ m with the superelevation 0.08 m, with the travelling speed value $v_0 = 49.2$ m/s $\cong 177$ km/h yielding the track excitation frequency $v_0/l_s = 82$ Hz, which corresponds to the smaller “peak” of the proper frequency response function shown in Fig. 8. The respective numerical results obtained for these examples are presented in Figs. 11 and 12. Since on the curved track the system dynamic responses for the left and right wheels do not overlay, the investigated quantities for the left wheels are also plotted, where the results for the left wheel of the first wheelset are depicted by the black dashed line and these for the left wheel of the second wheelset are depicted by the grey dashed line.

The centrifugal force action during run on the left curve presses down the outer right wheels to the rail and releases the inner left wheels of the bogie, which results in greater average vertical wheel-rail contact force values for the right wheels and in smaller average vertical contact force values for the left wheels in comparison with the nominal static gravitational force on the straight track without any superelevation, Figs. 11 and 12. Moreover, due to stronger parametric excitation from the track, the contact force fluctuation amplitudes for the right wheels pressed down are slightly greater than those for the released left

wheels with the common track excitation frequencies $v_0/l_s = 126$ and 82 Hz, respectively, for $v_0 = 272$ and 177 km/h. Similarly as for the bogie motion on the straight track, on the curved one with the travelling speed $v_0 = 272$ km/h, the fluctuations of the vertical wheel-rail dynamic contact forces for the first wheelset are greater than those for the second one. Hence, in this case, the first wheelset is also dynamically pressed down and the second one is dynamically released. However, for $v_0 = 177$ km/h one can observe that the second wheelset is dynamically pressed down and the first one is dynamically released, which results in respectively very significant differences of the corresponding wheel-rail vertical contact force amplitudes shown in Figs. 11 and 12.

Lack of the differential mechanism in railway wheelsets results on the curved track in essential constant components of the tangential wheel-rail contact forces in the longitudinal direction. These forces yield large static components of the dynamic torques transmitted by the wheelset axles and of the wheel longitudinal displacements, i.e. positive for the accelerated left wheels and negative for the braked right wheels. The absolute values of static torque components reach ~ 750 Nm for $v_0 = 272$ km/h at $R_0 = 4000$ m, Fig. 11, and ~ 1500 Nm for $v_0 = 177$ km/h at $R_0 = 1800$ m, Fig. 12. They are much greater than their amplitudes of fluctuation. Nevertheless, fluctuations of the longitudinal displacements of the left and right wheels as well as of the dynamic torques transmitted by the wheelset axles between the wheels and the adjacent brake disks are remarkably greater than those obtained for the straight track. Particularly for $v_0 = 177$ km/h it should be remarked that for all the considered dynamic torque histories, the components of track excitation of frequency $v_0/l_s = 82$ Hz are comparable to the excitation components due to the unbalances, contrary to the case of the straight track, for which excitation due to the unbalances is of primary importance, as it follows from the proper results of the fast Fourier transformation. However, for $v_0 = 272$ km/h on the straight and curved track the influence of the track parametric excitation, in comparison with the excitation due to the unbalances, is not so essential as for $v_0 = 177$ km/h, Figs. 10 and 12. For the left- and right-hand wheels different values of the vertical and longitudinal average forces acting during the run on the curved track result in respectively different constant vertical and longitudinal components of the dynamic displacements of the wheel centers, which demonstrate the completely different orbits for the left and right wheels presented in Figs. 11 and 12. From the wheel center displacement orbits in Figs. 11 and 12 it also follows that on the curved track, similarly as on the straight one, the vertical vibration amplitudes are slightly greater for the wheels of the first wheelset for $v_0 = 272$ km/h, while for $v_0 = 177$ km/h the respective vertical displacement fluctuation amplitudes of the wheel centers of the first wheelset are much smaller than those of the second one.

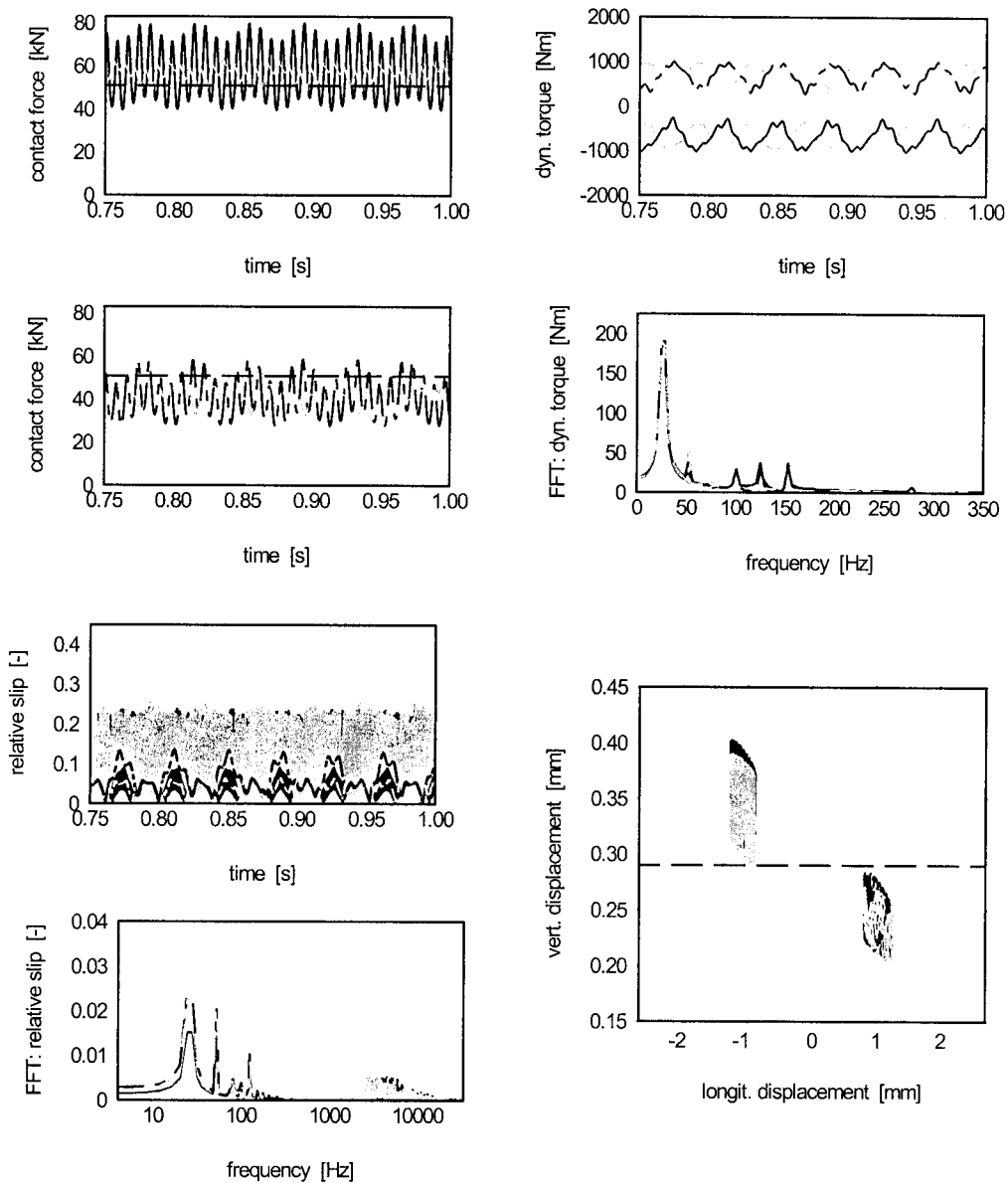


FIG. 11. Dynamic response of the bogie-track system for the curved "hard" track with a radius of curvature of 4000 m for $v_0 = 272$ km/h; (—) - for the right-hand wheel of the 1st wheelset, (---) - for the right-hand wheel of the 2nd wheelset, (- - -) - for the left-hand wheel of the 1st wheelset, (- · - ·) - for the left-hand wheel of the 2nd wheelset, (— · — ·) - for the static values.

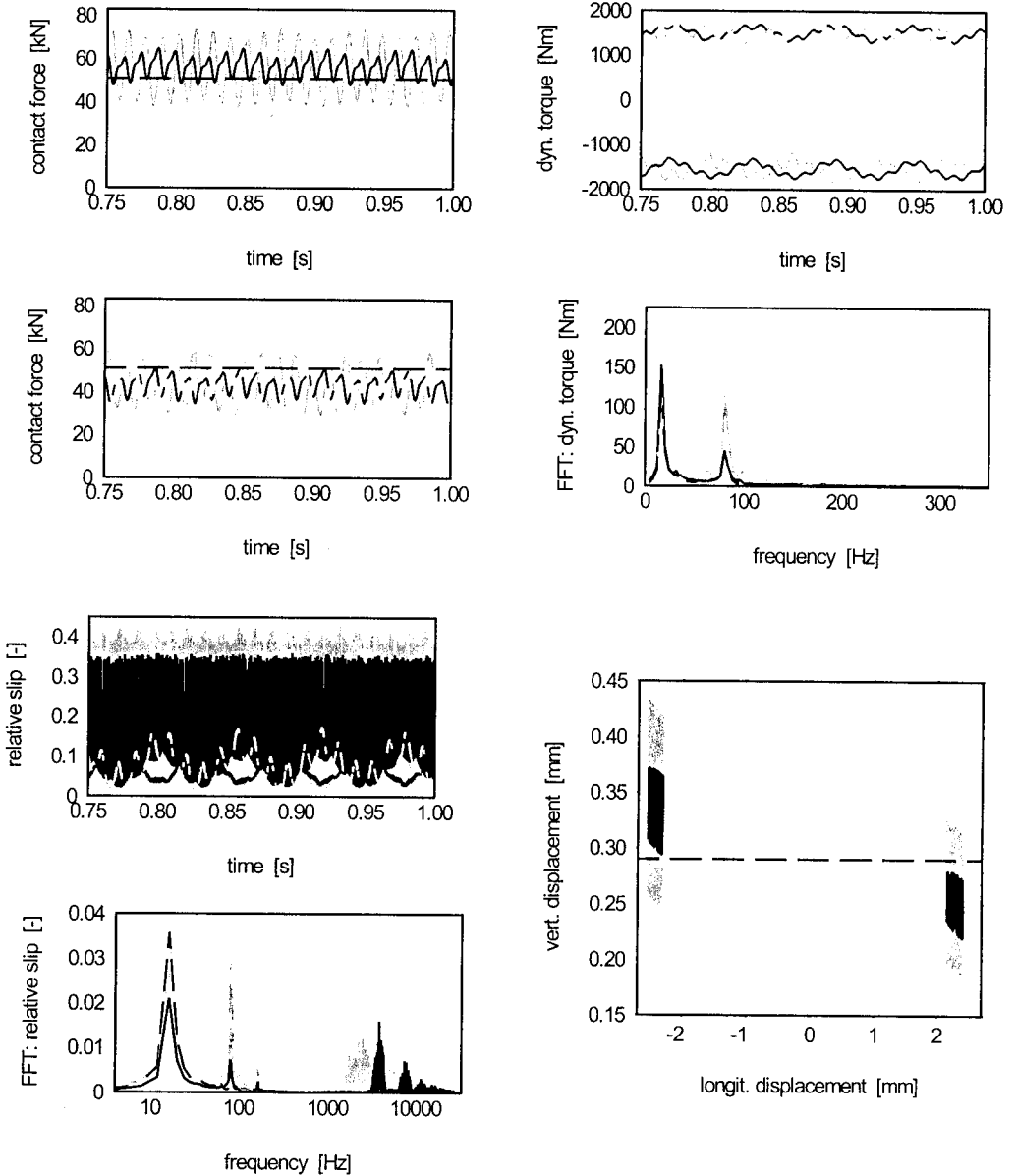


FIG. 12. Dynamic response of the bogie-track system for the curved "hard" track with a radius of curvature of 1800 m for $v_0 = 177$ km/h; (—) - for the right-hand wheel of the 1st wheelset, (····) - for the right-hand wheel of the 2nd wheelset, (- - -) - for the left-hand wheel of the 1st wheelset, (- · - ·) - for the left-hand wheel of the 2nd wheelset, (— — — —) - for the static values.

In all the above considered computational examples, both on the straight and the curved track, the quantity of particular interest are the resultant tangential wheel-rail slips related to the full slip value corresponding here to unity in accordance to [5, 15]. For the bogie runs on the straight track, the wheel-rail tangential slips for all the wheels are relatively small not exceeding 13% of the full slip value for $v_0 = 272$ km/h and 8% for $v_0 = 177$ km/h. Both tangential slips are characterized by “smooth” time histories, which fluently oscillate around the ca. 7.5 and 5% constant component values respectively for $v_0 = 272$ km/h and $v_0 = 177$ km/h, Figs. 9 and 10. This means that on the straight tracks, the bogie interacts with the track within the range of the so-called “micro-slips”. From the fast Fourier transformation (FFT) of the relative slip time histories obtained for the straight track it follows that, beyond the excitations due to the residual wheelset unbalances and the track property fluctuation, the component of double unbalance frequency, i.e. $2\Omega/(2\pi)$, is predominant, Figs. 9 and 10. This fact can be explained by a character of coupling between the wheelset torsional and bending vibrations in the longitudinal direction, which significantly influence the wheel-rail slips. According to the assumptions for the considered bogie-track system, this coupling is caused by the wheel-rail tangential contact effects and by the wheelset residual unbalances described by the boundary conditions (3.2). In Figs. 9 and 10 the former is expressed by the component of the track excitation frequency v_0/l_s , and the latter by the so-called synchronous $\Omega/(2\pi)$, and double synchronous frequency $2\Omega/(2\pi)$, which follows from the respective terms in Eq. (3.2)₅. In Figs. 11 and 12 demonstrating simulation results for the bogie running on the curved track, the time histories of the slips for the, inner in the left curve, left wheels are similar to those for the straight track. However, for the outer right wheels, the resultant tangential slips are characterized by quite regular successive large “peaks”, the maximum values of which for $v_0 = 272$ km/h and $R_0 = 4000$ m slightly exceed 0.25, and for $v_0 = 177$ km/h and $R_0 = 1800$ m they reach 0.45 of the full slip value equal to 1. This fact gives reason for the application of the non-linear Kalker’s theory in the assumed bogie-track model. For both the considered train speed values v_0 , the respective amplitude spectra are very “dense” and contain several high frequency components irregularly distributed along the whole frequency range $0 \div 33000$ Hz analyzed, which follows from the proper results of the fast Fourier transformation. The “peaky” time histories for the right wheel slips are caused by the lateral bogie-track interaction due to the centrifugal forces in the form analogous to the well known “stick-slip” effects for rigid bodies in a tangential contact. Due to the irregular character of this interaction mentioned above, a further qualitative analysis of these responses from the viewpoint of chaotic motions seems to be worth performing.

5. FINAL REMARKS

In the paper, a discrete-continuous mechanical model of the modern railway passenger car bogie interacting with a track was considered. By using this model it was possible to investigate the bending-torsional-lateral vibrations of the wheelsets coupled with vertical and lateral vibrations of the track. The proposed model is characterized by simple equations of motion for the wheelset axle cross-sections, where all the nonlinear and parametric terms describing excitation due to contact forces, unbalance effects and interactions with the supports are contained in the boundary conditions. The boundary conditions are coupled with ordinary differential equations which describe the motion of the track model and the bogie lateral vibrations. Solving the differential eigenvalue problem of the linearized system and application of the Fourier solutions in the form of series, lead to independent modal equations in the Lagrange coordinates. These equations are then mutually coupled by the parametric, nonlinear and gyroscopic terms regarded as external excitations expanded in series in the analytical eigenfunctions. Fast convergence of the Fourier solutions applied for the proposed approach enabled us to reduce the appropriate number of the modal equations to solve, in order to obtain a sufficient accuracy of results in the given range of frequency. Such a mathematical description of the investigated bogie-track model is formally strict, demonstrates clearly the qualitative system properties and is very convenient for a stable and efficient numerical simulation.

Comparison of the results of simulation obtained for the bogie motion on the straight track with those obtained on the curved track indicates the same qualitative character of the system response, but essential quantitative differences of the extreme as well as of the average values of the dynamic forces, torques, relative slips and displacements. In the paper an idealized system has been considered, i.e. the wheelsets with perfectly round wheels and the track with even uncorrugated rails. The purpose of such investigations was to search primary sources of dynamic interaction between the bogie and the track in the medium frequency range. From the obtained numerical results it follows that the periodic fluctuation of track properties during a run is a source of severe parametric excitation, leading to the essential increase of fluctuation amplitudes of the vertical wheel-rail dynamic contact forces, which can cause local plastic deformations on the wheel treads and start the polygonalization process. Nevertheless, introduction of kinematic excitations due to rail and wheel tread unevenness to the proposed model of the bogie-track system makes no difficulties.

In the numerical examples presented, the essential influence of the track dynamic and static properties on the extreme values of dynamic wheel-rail vertical contact forces and tangential slips has been demonstrated. From the results ob-

tained for the considered passenger car bogie running on the "soft" track with wooden sleepers as well as on the "hard" and "very hard" track with concrete sleepers, one can conclude that the character of dynamic bogie-track interaction is very complex and depends on numerous parameters of the given bogie and the track. From the analysis of the linearized bogie-track system in the form of frequency response functions it follows that in some frequency ranges, the given bogie can be more sensitive to vibrations and in the other ranges less sensitive, regardless of the dynamic and static track properties. Moreover, the strongly non-linear character of the wheel-rail contact creating the unilateral constrains qualitatively influences the system dynamic behaviour. Thus, it is impossible to foresee in advance the extreme values of the wheel-rail dynamic contact forces and tangential slips, dynamic torques transmitted by the wheelset axles and other quantities of interest, without thorough and detailed linear and non-linear dynamic analysis of the given bogie running on the given type of the track for various kinds and magnitudes of excitations. The presented mechanical and mathematical model of the bogie track-system enables us to perform such analyses in a wide range of parameters of the bogie and of the straight and curved tracks.

ACKNOWLEDGEMENT

This work has been financially supported by the Polish Research Council (KBN) – Project No. 9 T12C 082 14.

APPENDIX

The coefficients of the orthogonality properties

– for system motion in the vertical plane:

$$\begin{aligned} \gamma_{Vm}^2 = & \sum_{l=1}^2 \left\{ m_1 U_{l1m}^2(0) + \sum_{i=2}^{n+3} \left[m_i U_{lim}^2(\lambda_i) + J_i \Phi_{lim}^2 \right] \right. \\ & + m_{n+4} U_{l,n+3,m}^2(\lambda_{n+4}) + \rho \sum_{i=1}^{n+3} A_i \int_{\lambda_i}^{\lambda_{i+1}} U_{lim}^2(y) dy + \hat{m}_{V11} Z_{11lm}^2 \\ & + \hat{m}_{V12} Z_{12lm}^2 + \hat{m}_{V2} \left(Z_{21Lm}^2 + Z_{21Rm}^2 \right) + \hat{m}_{V3} \left(Z_{31Lm}^2 + Z_{31Rm}^2 \right) \left. \right\} \\ & + m_{Z1} \left[Z_{Lm}^2 + Z_{Rm}^2 \right] + 2m_{Z2} [Z_{Lm} Z_{Rm}] + I_y A_{Bm}^2, \end{aligned}$$

where

$$m_{Z1} = \frac{1}{4}m_{A5} + \frac{I_x}{a^2}, \quad m_{Z2} = \frac{1}{4}m_{A5} - \frac{I_x}{a^2},$$

– for system motion in the longitudinal direction:

$$\begin{aligned} \gamma_{Hm}^2 = \sum_{l=1}^2 \left\{ m_1 W_{l1m}^2(0) + \sum_{i=2}^{n+3} [m_i W_{lim}^2(\lambda_i) + J_i \Psi_{lim}^2] \right. \\ \left. + m_{n+4} W_{l,n+3,m}^2(\lambda_{n+4}) + \rho \sum_{i=1}^{n+3} A_i \int_{\lambda_i}^{\lambda_{i+1}} W_{lim}^2(y) dy \right\} \\ + m_{X1} [X_{Lm}^2 + X_{Rm}^2] + 2m_{X2} [X_{Lm} X_{Rm}] \end{aligned}$$

where

$$m_{X1} = \frac{1}{4}m_{A5} + \frac{I_z}{a^2}, \quad m_{X2} = \frac{1}{4}m_{A5} - \frac{I_z}{a^2},$$

– for torsional motion of the wheelsets:

$$\begin{aligned} \gamma_{Tm}^2 = \sum_{l=1}^2 \left\{ I_{01} \Theta_{l1m}^2(0) + \sum_{i=2}^{n+3} I_{0i} \Theta_{lim}^2(\lambda_i) + I_{0,n+4} \Theta_{l,n+3,m}^2(\lambda_{n+4}) \right. \\ \left. + \rho \sum_{i=1}^{n+3} J_{0i} \int_{\lambda_i}^{\lambda_{i+1}} \Theta_{lim}^2(y) dy \right\}, \quad m = 1, 2, \dots, \end{aligned}$$

– for lateral motion of the track:

$$\begin{aligned} \gamma_{Lm}^2 = \sum_{l=1}^2 \left\{ \hat{m}_{L1} Y_{l1m}^2 + \hat{m}_{L2} [(Y_{2lLm} + s_o Y_{4lLm})^2 \right. \\ \left. + (Y_{2lRm} + s_o Y_{4lRm})^2] + \hat{m}_{L3} [(Y_{3lLm} + s_o Y_{4lLm})^2 \right. \\ \left. + (Y_{3lRm} + s_o Y_{4lRm})^2] + \hat{m}_{L4} (Y_{4lLm}^2 + Y_{4lRm}^2) \right\}, \quad m = 1, 2, \dots, 7, \end{aligned}$$

– for lateral motion of the bogie:

$$\gamma_{Am}^2 = m_{A5} Y_{5Bm}^2 + \sum_{l=1}^2 \left\{ m_A (Y_{6lLm}^2 + Y_{6lRm}^2) + m_{A7} Y_{7lWm}^2 \right\},$$

$$m = 1, 2, 3, 4,$$

where $\lambda_i = \sum_{j=1}^{i-1} l_j$, and \hat{m}_{tk} , $k = 1, 2, 3$ for $t = V$, $k = 1, 2, 3, 4$ for $t = L$, are the mean values of mass parameters of the track model determined by the first components of the sums in (2.2), $m_A = m_2 = m_{n+3}$ are masses of the rigid rings representing wheels, m_{A5} denotes the mass of the bogie frame, and m_{A7} is the total mass of the wheelset axle and n brake disks, I_x, I_y, I_z denote respectively the mass moments of inertia of the bogie frame with regard to the main axes x, y, z , and $X_{Lm}, X_{Rm}, Z_{Lm}, Z_{Rm}, A_{Bm}$ are the eigenvector components of the generalized coordinates describing vertical and longitudinal motion of the rigid body (5B).

REFERENCES

1. J. KISILOWSKI, and K. KNOTHE, *Advanced railway vehicle system dynamics*, WNT, Warsaw 1991.
2. J.-P. PASCAL and G. SAUVAGE, *Theoretischer Vergleich des dynamischen Verhaltens eines Hoch-geschwindigkeits-Drehgestells mit verschiedenen Radprofilen auf Schienen des Types UIC 60 mit einer Einbauneigung von 1/20 bzw. 1/40.*, Systemdynamik der Eisenbahn, VDI Fortschritt-Berichte, **820**, 11-24, 1990.
3. U. FINGBERG, *Ein Modell für das Kurvenquietschen von Schienenfahrzeugen*, VDI Fortschritt-Berichte, Reihe **11**, 140, 1990.
4. U. FINGBERG and K. POPP, *Experimentelle und theoretische Untersuchungen zum Schallabstrahlverhalten von Schienenrädern*, Deutsche Forschungsgemeinschaft (DFG), Final Report Po 136/5-2, August 1991.
5. K. POPP and W. SCHIEHLEN, *Fahrzeugdynamik*, [Ed.] B. G. TEUBNER, Stuttgart 1993.
6. J.-P. PASCAL and G. SAUVAGE, *The available methods to calculate the wheel/rail forces in non-Hertzian contact patches and rail damaging*, Vehicle System Dynamics, **22**, 263-275, 1993.
7. R. BOGACZ, P. MEINKE and K. POPP, *Zur Modellierung der höherfrequenten Radsatz/Gleisdynamik*, Hestra Verlag: Report on the *Tagung Systemdynamik der Eisenbahn*, 13-14 Oct. 1994 in Henningsdorf, Germany, 45-55, 1994.
8. B. RIPKE, *Hochfrequente Gleismodellierung und Simulation der Fahrzeug-Gleis-Dynamik unter Verwendung einer nichtlinearen Kontaktmechanik*, VDI Fortschritt-Berichte, Reihe **12**, 249, 1995.
9. G.-K.-W. VOHLA, *Werkzeuge zur realitätsnahen Simulation der Laufdynamik von Schienenfahrzeugen*, VDI Fortschritt-Berichte, Reihe **12**, 270, 1996.
10. K. POPP, H. KRUSE and I. KAISER, *Vehicle-track dynamics in the mid-frequency range*, Vehicle System Dynamics, **31**, No. 5-6, 423-464, 1999.
11. K. HEMPELMANN and K. KNOTHE, *Eigenschwingungsberechnung von Radsätzen mit statisch optimalen Ansatzfunktionen*, VDI Fortschritt-Berichte, Reihe **11**, No. 114, 1989.

12. T. SZOLC, *Medium frequency dynamic investigation of the railway wheelset-track system using a discrete-continuous model*, Archives of Applied Mechanics (Ingenieur Archiv), **68**, 1, 30–45, 1998.
13. T. SZOLC, *Simulation of bending-torsional-lateral vibrations of the railway wheelset-track system in the medium frequency range*, Vehicle System Dynamics, **30**, 6, 473–508, 1998.
14. T. KRZYŻYŃSKI, *On dynamics of track modeled as two-dimensional periodic structure*, Proc. 4th Engineering Foundation Conference on Vehicle-Infrastructure Interaction, San Diego, USA, June 1996.
15. J. ZHANG and K. KNOTHE, *Berechnungsmodell für Tangentialschlusskräfte beim Kontakt in der Hohlkehle*, Report of the Institut für Luft- und Raumfahrt der Technischen Universität Berlin, ILR-Mitteilung, **294**, 1995.

Received January 13, 2000; revised May 23, 2000.
